

AUTOMATED DATA-DRIVEN DESIGN AND OPTIMIZATION OF BONE SCAFFOLDS USING MACHINE LEARNING AND COMPUTATIONAL ANALYSIS

21ME810 - PROJECT

Submitted by

HARIPRASATH H S (917721G027)

RAJESHKUMAR B (917721G077)

VEJEY MAHEAS RAAJHAA MU (917721G110)

*in partial fulfillment of the requirements for B.E. degree in Mechanical
Engineering of Anna University*

Guided by

Dr. M. Karthic

Assistant Professor



**Department of Mechanical Engineering
THIAGARAJAR COLLEGE OF
ENGINEERING**

(A Govt. Aided Autonomous Institution Affiliated To Anna University)

MADURAI-625 015

MAY 2025

THIAGARAJAR COLLEGE OF ENGINEERING
(A Govt. Aided Autonomous Institution Affiliated To Anna University)

MADURAI-625 015



BONAFIDE CERTIFICATE

Certified that this is a Bonafide record of the 21ME810 Project Work & Viva Voce done by **Mr. HARIPRASATH H S (917721G027)**, **Mr. RAJESHKUMAR B (917721G077)** and **Mr. VEJEY MAHEAS RAAJHAA (917721G110)** of Eight Semester B.E. (Mechanical Engineering) during the year 2024 - 2025.

M. Kauthir
7/5/25
Signature of the Guide

Ravi
~ 07/05/25
Signature of HDME

Station: Madurai
Date: 07/05/2025

Submitted for Viva-voce Examination held at Thiagarajar College of Engineering, Madurai – 625 015, on 07/05/2025.

M. Kauthir
INTERNAL EXAMINER

[Signature]
7.5.2025
EXTERNAL EXAMINER

[Signature]
HDME

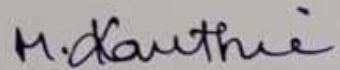
CERTIFICATE

This is to certify that the 21ME810 Project Report entitled "AUTOMATED DATA-DRIVEN DESIGN AND OPTIMAZATION OF BONE SCAFFOLD USING MACHINE LEARNING AND COMPUTATIONAL ANALYSIS", being submitted **Mr. HARIPRASATH HS (917721G027), Mr. RAJESHKUMAR B (917721G077) AND Mr. VEJEY MAHEAS RAAJHAA (917721G110)** in partial fulfillment of the requirement for Bachelor of Engineering Degree in Mechanical Engineering, is a record of Bonafede work. The results embodied in this report have not been submitted to any other university or institute for the award of any degree or diploma.



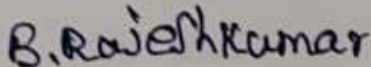
Student Signature

Mr. HARIPRASATH H S



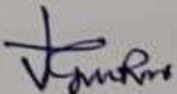
Guide Signature

Dr. M KARTHIC



Student Signature

Mr. RAJESHKUMAR B



Student Signature

Mr. VEJEY MAHEAS RAAJHAA

Station: Madurai

Date: 7/5/2025

ACKNOWLEDGEMENT

We would like to express our gratitude to the members who were all supportive to complete our project successfully.

We extend our hearty thanks to the principal **Dr. L. Ashok Kumar**, for giving great support and encouragement towards our project.

We are grateful to head of the department in mechanical engineering **Dr. K. Srithar, Professor** for his encouragement, guidance and technical support towards our project.

We express our sincere thanks to our project guide, **Dr. M. Karthic, Assistant Professor** of Mechanical Engineering for being backbone throughout the project by guiding us in the right way whenever we went wrong and providing additional ideas to complete this project successfully.

We are grateful to our reviewers, **Dr. PL. K. Palaniappan** and **Dr. M. Karthic** for their continuous support and for the corrections they made throughout our whole project.

We thank all other **Faculty members & Supporting staff members** of the Department of Mechanical Engineering for indirectly helping and supporting us to complete this project successfully. We extend special thanks to our **Parents** who have supported and motivated us in our education and supported us financially as well.

Mr. HARIPRASATH H S

Mr. RAJESHKUMAR B

Mr. VEJEY MAHEAS RAAJHAA

LIST OF CONTENTS

CHAPTER NO.	CONTENT	PAGE NO.
	TITLE PAGE	i
	BONAFIDE CERTIFICATE	ii
	CERTIFICATE	iii
	ACKNOWLEDGEMENT	iv
	LIST OF CONTENTS	v
	LIST OF SYMBOLS	ix
	LIST OF FIGURES	x
	LIST OF TABLES	xii
	ABSTRACT	xiii
1	INTRODUCTION	1
1.1	INTRODUCTION	1
1.2	BONE BASICS	1
1.3	BONE STRUCTURE	2
1.4	HUMAN BONE CELLS	2
1.5	BONE DEFECTS AND CURRENT TREATMENT OPTIONS	3
1.6	TISSUE ENGINEERING	4
1.7	COMPONENTS OF TISSUE ENGINEERING	4
1.8	TYPES OF TISSUE ENGINEERING	5
1.9	APPLICATIONS OF TISSUE ENGINEERING	6
1.10	BONE TISSUE ENGINEERING	6
1.11	MARKET SURVEY	7
2	LITERATURE REVIEW	8
2.1	PREAMBLE TO LITERATURE REVIEW	8
2.2	LITERATURE REVIEW	8
2.3	INFERENCE FROM LITERATURE REVIEW	17
3	PROBLEM DESCRIPTION	
3.1	BONE DEFECT AND LOSS	19
3.2	PROBLEM STATEMENT	19

CHAPTER NO.	CONTENT	PAGE NO.
3.3	OBJECTIVE	19
4	METHODOLOGY	21
4.1	WORKFLOW METHODOLOGY OF THE PROJECT	21
5	EXPERIMENTAL SETUP	23
5.1	SCAFFOLD DESIGN AND GENERATIONS	23
5.1.1	Parameters	23
5.1.2	Available Length for Holes	23
5.1.3	Spacing between pores	24
5.1.4	Wall thickness check	24
5.1.5	Recommended Number of Holes	24
5.1.6	Hole center positions	25
5.2	PORE SHAPES	25
5.2.1	Pore area	25
5.3	STRUCTURE CREATIONS	25
5.3.1	Openscad structure creations	26
5.3.2	Cadquery structure creations	26
5.3.3	Structure automation	27
5.4	POROSITY CALCULATION	28
5.4.1	Porosity	28
5.4.2	Solid volume	28
5.4.3	Total volume	28
5.4.4	Surface area	29
5.4.5	Porosity automation	29
5.5	DESIGN OF SCAFFOLD	30
5.5.1	Square pore scaffold	30
5.5.2	Circle pore scaffold	30
5.5.3	Hexagon pore scaffold	31
5.5.4	Pentagon pore scaffold	31
5.5.5	Diamond pore scaffold	31
5.6	FABRICATION OF SCAFFOLD	32

CHAPTER NO.	CONTENT	PAGE NO.
5.6.1	Fabrication of scaffolds by FDM	32
5.6.2	Square, circular, hexagonal, diamond and pentagon pore scaffold	33
5.7	FEA ANALYSIS	36
5.7.1	File conversion	36
5.7.2	Ansys simulations	36
5.8	MACHINE LEARNING APPROACH	36
5.9	EXPERIMENTAL SETUP	37
5.9.1	Archimedes porosity measurement	38
5.9.2	Compression test	38
5.9.3	Permeability analysis	39
6	RESULTS AND DISCUSSIONS	40
6.1	FEA RESULTS	40
6.2	POROSITY ANALYSIS	45
6.3	COMPRESSION BEHEVIOR	47
6.3.1	Structure properties relationship	49
6.4	MACHINE LEARNING MODELS	50
6.4.1	Porosity prediction	50
6.4.2	Permeability prediction	53
6.4.3	Number of pore predictions	56
6.4.4	FEA predictions	67
7	CONCLUSION	60
	REFERENCES	61

LIST OF SYMBOLS

SYMBOL	DESCRIPTION
PLA	Poly lactic acid
FDM	Fused deposition modelling
L_x	Cube width
L_y	Cube breadth
L_z	Cube height
D_p	Pore diameter
t_{outer}	Margin (outer thickness)
N_x	Number of holes in width direction
N_y	Number of holes in breadth direction
N_z	Number of holes in height direction
A	Available spaces in cube after margin
S	Specing width between two pores
t_x	Wall thickness
t_{min}	Minimum wall thickness
SHAPE	Pore shape
A_p	Pore area

LIST OF FIGURES

FIGURE NO.	DESCRIPTION	PAGE NO.
1.1	Basic bone structure	2
1.2	Bone forming cells	3
1.3	Components of bone tissue engineering	5
1.4	Bone tissue engineering process	7
4.1	Workflow of our project	22
5.1	Pore shapes	26
5.2	The Tkinter interface for a structure automation	29
5.3	Tkinter Gui For Porosity Calculation	31
5.4	Square Pore Scaffold	31
5.5	Circle Pore Scaffold	32
5.6	Hexagon pore scaffold	32
5.7	Pentagon pore scaffold	33
5.8	Diamond pore scaffold	33
5.9	Fabricated Square scaffold	34
5.10	Fabricated Circle scaffold	34
5.11	Fabricated Hexagon scaffold	35
5.12	Fabricated Diamond scaffold	35
5.13	Fabricated Pentagon scaffold	35
5.14	Porosity measurement setup	38
5.15	BISS Nano Test system BI-7000 Machine	39
5.16	Before and After compression testing	40
6.1	FEA Results	43
6.2	Equivalent Stress and porosity	44

FIGURE NO.	DESCRIPTION	PAGE NO.
6.3	Max Principal Stress and porosity	44
6.4	Equivalent Strain and porosity	45
6.5	Max Deformation and porosity	45
6.6	Pore shape vs porosity	47
6.7	Load vs displacement	50
6.8	Stress Vs Strain	51
6.9	Pore Shape vs Compression strength and Modulas	51
6.10	Shape vs porosity and compression strength	52
6.11	Actual vs predicted porosity plot	54
6.12	Residual vs predicted porosity plot	54
6.13	Porosity model performance plot for test and train	55
6.14	Porosity model performance plot for test and train	55
6.15	Actual vs predicted Permeability	56
6.16	model performance plot for Permiability test and train	57
6.17	Actual vs predicted Permeability for test	57
6.18	Model performance plot for Permiability test	58
6.19	Model Average performance for training no. of pores	59
6.20	Model Average performance for testing no. of pores	59
6.21	R2 heat map	61
6.22	a) R2 score b) RMSE SCORE	61

LIST OF TABLES

TABLE NO.	DESCRIPTION	PAGE NO.
6.1	FEA RESULTS OF PORE DIA 1MM	42
6.2	ACTUAL POROSITY	48
6.3	THEORITICAL POROSITY	48
6.4	EXPRIMENTAL RESULTS OF SCAFFOLD GEOMETRY ON POROSITY AND MECHANICAL PROPERTIES	49

ABSTRACT

Bone scaffolds play a critical role in regenerative medicine, providing cell growth, nutrient supply, and vascularization for new bone formation. To function, a scaffold must achieve the balance of enough porosity to facilitate biological integration and strength to resist physiological loading, which may be difficult. Here, we introduce an integrated method for the optimization of bone scaffold design based on automated computer-aided design (CAD), finite element analysis (FEA), and machine learning (ML). We created 2,000 diverse scaffold designs based on varying cube and pore sizes, margin sizes, and port numbers, with various pore shapes such as squares, circles, hexagons, pentagons, and diamonds. CAD generation was done automatically using Python scripts, while porosity was computed based on the Trimesh library. Iron Python was employed to automate conversion from STL to STEP files, importation of geometry into ANSYS Workbench, meshing, application of boundary conditions, and mechanical simulations. Experimental confirmation was performed using 3D printed scaffolds (size: $12.7 \times 12.7 \times 25.4$ mm, pore size: 1 mm, pore arrangement: $5 \times 5 \times 12$). Measured porosity was 38.48%, which was near the simulated porosity of 37.23%. Compressive strength ranged from 10 to 16 MPa based on pore shape. We used linear as well as nonlinear models for the prediction of porosity, permeability, FEA output, and pore count. The support vector machine (SVM) gave an R^2 value of approximately 0.99 for porosity prediction with very less errors, whereas XGBoost and random forest models were applied for the prediction of permeability and FEA. This automated system presents a solution to the problem of designing bone scaffolds that meet mechanical strength and biological compatibility. In the near future, we plan to integrate the design process by enabling the user to select target properties such as porosity or compressive strength, diminishing the necessity of costly experiments. We also wish to improve the system by incorporating biological aspects such as cell growth behavior and anatomical modeling by medical imaging so that we develop personalized scaffold designs for individual patients.

CHAPTER 1

INTRODUCTION

1.1. INTRODUCTION

Bone tissue engineering plays a crucial role in regenerative medicine, addressing the growing demand for effective treatments of bone defects caused by trauma, disease, or congenital abnormalities. Traditional scaffold design methods often rely on trial-and-error approaches, which are time-consuming and may not always yield optimal results. To overcome these limitations, this project explores the integration of machine learning and computational analysis in the automated design and optimization of bone scaffolds. By leveraging data-driven techniques, we aim to develop an intelligent framework that can systematically generate, evaluate, and refine scaffold structures to enhance their biological and mechanical performance.

The key focus of this study is to create customizable and patient-specific bone scaffolds that promote better tissue regeneration, ensuring structural integrity, porosity, and mechanical strength tailored to individual needs. The project employs computational simulations to assess scaffold properties and machine learning models to optimize design parameters, making the process more efficient and accurate. By automating scaffold generation and optimization, this research contributes to advancements in personalized medicine, reducing the dependency on manual interventions and accelerating the transition from design to clinical applications. This report details the methodologies used, including data-driven modelling, simulation techniques, and optimization strategies, along with the anticipated impact of this approach in revolutionizing bone tissue engineering.

1.2. BONE BASICS:

Bones provides the structural support to our body, protects our organs by enclosing it in the structure. Inside the bone, bone marrow is present where blood cells are created and act as a storage reservoir for minerals and calcium. There will be a total of 270 bones present during birth where it reduces to 206 bones by fusing with each other during body growth. The largest and the smallest bone in the human body is the thighbone (femur) and the stapes in the ear respectively.

1.3. BONE STRUCTURE:

Bones are composed of two types of tissue

Compact (cortical) bone - It is present on the outer layer which is harder, stronger and denser as well and helps for our mechanical function

Cancellous (trabecular/spongy) bone – This type consists of trabeculae arranged in a network form. It is less dense and lighter than the cortical bone and helps in carrying out metabolic activities.

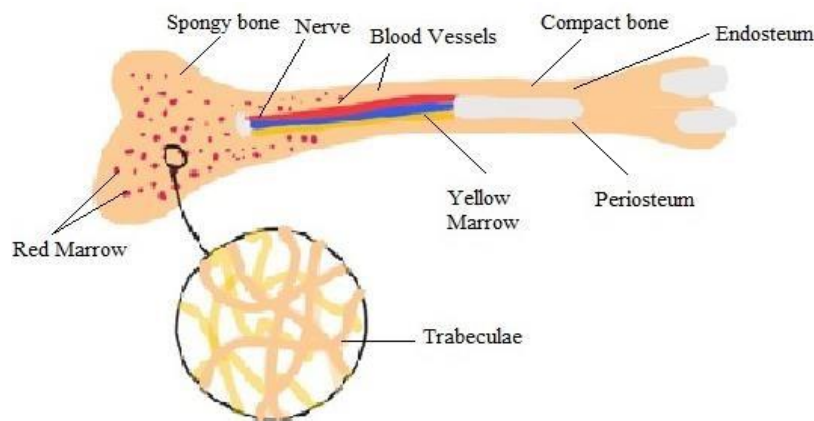


Figure 1.1 Basic bone structure

The other things found in bones include osteoblasts and osteocytes which helps in formation of bone, osteoclasts which help in resorption, osteoid which is a mix of proteins and collagen, inorganic mineral salts in the extracellular matrix, the bone marrow, cartilage tissue, endosteum and periosteum membranes. The basic bone structure explained as shown in **figure 1.1**.

1.4. HUMAN BONE CELLS:

There are three main cell types involved in the constant bone remodelling process

Osteoblasts: They are useful in the formation of new bones and helps in the process of repairing older bones. Osteoid, a protein and collagen mixture produced by osteoblasts which mineralizes and leads to the bone and bone matrix formation.

Osteocytes: They help in maintaining the bone tissue. The osteoblasts which are inactive gets entrapped within the bone created by them. They are interconnected with osteoblasts and other osteocytes.

Osteoclasts: They help in breaking down the bone. They help in dissolving the minerals by releasing the enzymes and digesting them which is called as the process of resorption of bone. They also help in remodelling process of injured bones as shown in **figure 1.2**.

Bone marrow: Bone marrow is present in the cancellous bone. They produce about 20 lakh red blood cells per second. They are also responsible for the production of white blood cells for immune response, platelets. The old and defective red blood cells are destroyed in the bone marrow.

Extracellular matrix: The extracellular matrix is composed of the organic components consisting of type 1 collagen and the inorganic components consisting of hydroxyapatite, calcium and phosphate salts. Collagen and hydroxyapatite give us the tensile strength and compressive strength to our bone respectively.

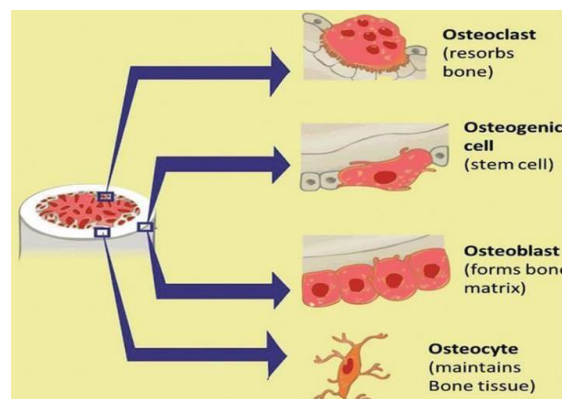


Figure 1.2 Bone forming cells

Source: Rosy Setiawati et.al 2018

1.5 BONE DEFECTS AND CURRENT TREATMENT OPTIONS:

Bone defects:

Bone defects may occur due to accidents, injuries such as the open fractures, debridement for nonunion (bone which is not healing) and developmental abnormalities.

It can also be caused due to surgical treatment of bone infection, tumors. Bone lesions is a medical condition when there is a loss of bone length occurring due to infection.

Current treatment options and their disadvantages:

The surgical methods include the bone transport distraction osteogenesis for treating developmental abnormalities and metallic bone implants. The bone grafting techniques includes allograft (graft from one individual to another of same species) and autograft (graft from one part to another part of the same individual). These existing treatment methods has many disadvantages because it leads to secondary damage, donor site injury, major deformity, morbidity and formation of scars due to grafts. These grafting and surgical techniques leads to bleeding and involves high cost and many surgeries. When larger volumes of grafts are required, autografts are not possible. To prevent all these risks, bone tissue engineering has been considered as one of the best alternate method to solve the bone defect problems.

1.6. TISSUE ENGINEERING:

Tissue engineering is a field of biomedical engineering that focuses on creating biological substitutes to repair, replace, or regenerate damaged tissues and organs. It combines principles from biology, engineering, and material science to develop functional tissues that mimic the properties of natural tissues in the human body.

1.7 COMPONENTS OF TISSUE ENGINEERING:

1. Cells

- Cells are the building blocks of tissues.
- They can be obtained from the patient (autologous), a donor (allogeneic), or stem cells.
- **Examples:** Stem cells, bone marrow cells, cartilage cells (chondrocytes), and skin cells (keratinocytes).

2. Scaffolds (3D Structures)

- Scaffolds provide a temporary structure for cells to attach, grow, and form new tissue.

- They must be **biocompatible**, meaning they should not cause immune reactions.
- Materials used:
 - **Natural** – Collagen, fibrin, alginate, chitosan.
 - **Synthetic** – Polylactic acid (PLA), polyglycolic acid (PGA), polycaprolactone (PCL).
 - **Hybrid** – A combination of natural and synthetic materials.

3. Growth Factors & Biochemical Signals

These are molecules that guide cell growth, division, and differentiation.

Examples: Bone Morphogenetic Proteins (BMPs) for bone growth, Vascular Endothelial Growth Factor (VEGF) for blood vessel formation as shown in **figure 1.3**.

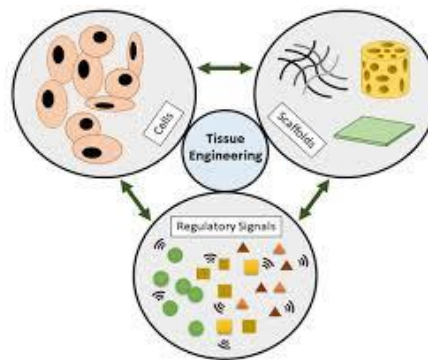


Figure 1.3 Components of bone tissue engineering

Source: Izzat Zulkiflee et.al and Fauzi Mb et.al

1.8 TYPES OF TISSUE ENGINEERING:

- Soft Tissue Engineering – Focuses on skin, muscle, cartilage, and ligaments.
- Hard Tissue Engineering – Involves bone and dental tissue regeneration.
- Organ Engineering – Aims to create kidneys, livers, hearts, and lungs.
- Neural Tissue Engineering – Focuses on brain, spinal cord, and nerve regeneration.
- Vascular Tissue Engineering – Develops artificial blood vessels for circulation repair.

1.9 APPLICATIONS OF TISSUE ENGINEERING:

1. Bone and Cartilage Repair

- Used to treat bone fractures, joint damage, and osteoporosis.
- **Bone scaffolds** (like the ones you are working on) provide a structure for bone cells to grow.

2. Skin Grafts & Wound Healing

- Artificial skin is used for burn victims and chronic wounds.
- Example: Apligraf (a bioengineered skin substitute).

3. Blood Vessel & Heart Tissue Engineering

- Artificial blood vessels for heart bypass surgeries.
- Engineered heart valves that reduce rejection risk.

4. Organ Regeneration (Kidney, Liver, Pancreas, etc.)

- Research is ongoing to create lab-grown organs to reduce transplant shortages.
- Example: 3D-printed mini-livers for drug testing.

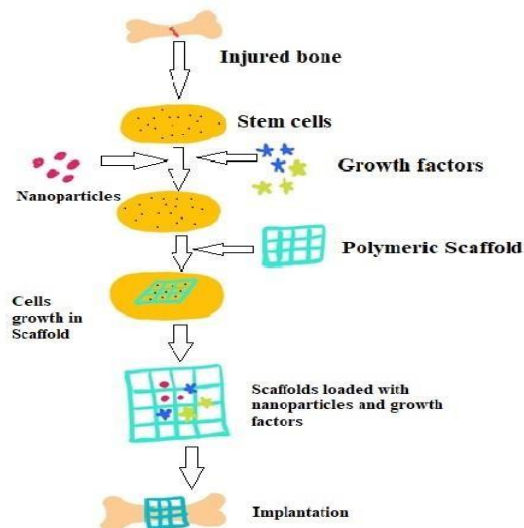
5. Nerve and Spinal Cord Repair

- Artificial nerve grafts help regenerate damaged nerve connections.
- Helps in treating spinal cord injuries and neurological disorders.

1.10 BONE TISSUE ENGINEERING:

Bone tissue engineering is a biomedical field that creates implantable bone substitutes for bone defects by the combination of cells, materials, methods, biochemical and physicochemical factors to improve, regenerate the damaged bone tissue region. It involves the use of scaffold where cells are placed and it leads to the formation of new tissue. The bone tissue engineering has vast range of applications involving the regeneration of damaged tissue and can be done in the areas of orthopaedics such as bones and joints. These defects can be due to orthopaedics, surgical treatments etc. The regeneration of tissue is done with the help of biomaterial scaffolds. The scaffolds are

made with polymeric biomaterials which can provide structural support for the cell attachment and bone tissue regeneration or development. Since our human body involves with variable forces the implantable scaffold should possess good mechanical properties. Bone tissue engineering process is depicted in figure 1.4.



Source: Yuan et al.

Figure 1.4 Bone tissue engineering process

1.11. MARKET SURVEY:

The bone defects in the legs are associated with injuries from sports, ageing, fractures, infections and trauma. European injury database suggests that an average of about 61 lakh people gets treatment in hospital for sports injuries in the European regions. The average cost for patients suffering from fractures from motorcycle accident estimated to be 10000 USD and nonunion cost about 25000 USD. The global bone graft and substitutes market size was about USD 2.78 billion in 2020 and it is expected to go about 4.3 billion USD growing at a Compound Annual Growth Rate of 5.8%. The bone graft and substitutes were normally based on allograft, autograft. But now there is an increasing market for synthetic biomaterial implants. Synthetic materials include composites, polymers, ceramics etc. The global market size of biomaterials in 2019 was estimated to be 106.5 billion USD and it was expected to grow up to 348.4 billion USD by 2027 at a compound annual growth rate of 15.9%.

CHAPTER 2

LITERATURE REVIEW

2.1 PREAMBLE TO LITERATURE REVIEW:

Bone Tissue Engineering (BTE) is emerging to help overcome the barriers of traditional bone grafts that rely on harvested tissue and donor grafts to build bone with a synthetic scaffold that balances mechanical requirements mechanical and biological function. The emergence of Additive Manufacturing (AM) has invented new designs for complex biomimetic structures - ranging from TPMS (Triply-Periodic Minimal Surfaces) to any number of increasingly complex structures - although reproducing the requisite scaffold properties remains limited. While computational modeling may help to inform scaffold design, the computational resources required can often limit usability unless done well in advance. Machine Learning promotes a robust alternative that offers faster prediction and design. The goal of this study is to combine the growth potential of ML with simulation techniques, allowing scaffold design to be automated to streamline the development of user-imagined, ultimate-performing biomaterials which facilitate personalized bone regeneration.

2.2 LITERATURE REVIEW:

Albano G *et al* (2019) conducted the Scaffolding Toolkit which highlights how to enhance students' argumentation and proof abilities in mathematics. The toolkit identifies ways to integrate digital and collaborative learning strategies with structured reasoning. The authors provided case studies which demonstrated how scaffolding strategies (guided prompts, discussion of peers, software) supported the organization of logical arguments and proofs, and thus aided students in constructing logical arguments and proofs. Overall, the authors concluded that structured support enhanced mathematical reasoning, along with the convenience and engagement of students' deeper thinking. The study reminds us that there are adaptive learning tools in the mathematics education experience which we can take advantage of and thus leverage technology to bridge abstract reasoning gaps. The journal utilized for this study is also reputable, with a focus in the education technology research community, often publishing articles to generate awareness of evidence based innovations in higher education. This remained consistent with the journal's overall goal to support educators engaging with ways to use digital tools

to reimagine/restage teaching and learning practices. For educators, the scaffolding perspective offers ideas of ways to create conditions for student that support and facilitate critical thinking in STEM disciplines.

Anja Conev *et al* (2020) says that, this study investigates how a Machine Learning (ML) approach can help minimize the amount of trial and error involved in 3D printing of tissue engineering scaffolds. Two ML methods, classification and regression, both based on Random Forests, are examined to assess their ability to predict quality of printed materials in a classification of low or high quality. Our findings indicate that the ML models accurately predict printing quality and outperform simpler linear models and allow us to understand where variations occur(e.g., the most significant variables were the material composition, printing speed and the pressure). Also, we provide an interesting debate on redundancy in data collection and present an alternative approach to progress.

Bandyopadhyay A *et al* (2021) says that, the revolutionary promise in medication delivery, tissue engineering, and customized treatment. The authors highlight the benefits of several 3D printing techniques, such as stereolithography (SLA), selective laser sintering (SLS), and fused deposition modeling (FDM), in producing implants, scaffolds, and prosthetics that are customized for each patient. The authors go on to address the difficulties encountered while implementing 3D printing, such as the materials' mechanical qualities, biocompatibility, and regulatory issues. With improved clinical results, the authors discussed developments in bioactive and biodegradable materials such composites, polymers, and ceramics. This article, which was published on March 1, 2023, in the prestigious materials science journal JMR, shows how biomaterials, 3D printing, and health innovation are closely related. Because JMR is a reputable journal that publishes high-caliber research, academics and industry professionals can trust this article.

Bouakaz I *et al* (2024) says that, examines the implementation of 3D printed hydroxyapatite (HA) scaffolds with a Gyroid-Triply Periodic Minim Surface (TPMS) porous structure to aid in bone regeneration. The researchers used advanced 3D printing techniques to fabricate HA scaffolds using a well interconnected porous architecture, mimicking the porous scaffold of a natural bone structure. An in vivo pilot sheep study demonstrated promising results by showing that the scaffolds had good biocompatibility,

osteoconductivity, and mechanical stability. The Gyroid-TPMS design improved bone ingrowth and vascularization compared to traditional porous structures.

Chao Wang *et al* (2021) says that, the study analyzed the most optimal pore configuration and size of porous Ti6Al4V scaffolds with both osteogenic and vascularization capabilities, both necessary for healing of large bone defects. Seven scaffold groups fabricated by Electron-beam melting (EBM) were evaluated on BMSC adhesion, proliferation, and differentiation.

Chi Wu *et al* (2024) says that, this project plan employs machine learning (ML) to enhance the optimization of ceramic additive manufacturing (AM) to improve tissue scaffolds made of Triply Periodic Minimal Surfaces (TPMS). The primary aim of the project is to optimize a BO (bayesian optimization) algorithm to optimize the design with optimal biomechanical properties to maximize conditions for bone regeneration. The LCM (lithography-based manufactured) fabrication process will be used, as this has the greatest precision to create anatomically correct bones with morphological porosities and immense mechanical strength. The scaffolds will be fully evaluated by micro-computed tomography (micro-CT) to examine the full geometric complexity of the designed scaffolds which will enable to confirm geometric complexity and structural integrity.

Elisa Rold'an *et al* (2024) says that, The aim of this research is to determine the similarities in mechanical properties between 2D and 3D electrospun polyvinyl alcohol (PVA) scaffolds, non-crosslinked and crosslinked. The research team used tensile testing and 28 predictive models, specifically utilizing Young's modulus and ultimate tensile strength to measure the scaffolds. This research wants to be able to identify similar structures to scaffolds of viable biological tissues to improve tissue-engineered implants development for future clinical uses.

Farina E *et al* (2021) says that, Elastic modulus and compressive strength were accurately predicted by the FEM approach, suggesting that the scaffold architecture—including pore size and distribution—influences mechanical performance. The study demonstrated that μ CT-based FEM is a practical tool for minimizing experimental expenses and optimizing scaffold design before production. The findings of this study can contribute to the development of bioactive glass scaffolds specifically designed for regenerative medicine and the harmony between porosity and mechanical integrity for cell proliferation. *Acta Mechanica Sinica*, which is published by the Chinese Society of

Theoretical and Applied Mechanics, is a perfect place for this study since it publishes high-impact mechanical research and welcomes contributions from all areas of mechanics. The study emphasizes how computer modeling advances the design of biomaterials.

Huang YZ *et al* (2020) says that the function of scaffolds for bone regeneration and repair. Scaffolds have some element of 3D structure to enhance cell growth, differentiation and ultimately tissue formation. These authors also provide a summary of progress in potential scaffold materials, which includes natural (e.g., collagen or chitosan) or synthetic polymers (e.g., PLA or PCL) and bioceramics (e.g., hydroxyapatite). It is of utmost importance that properties like porosity, mechanical strength and biodegradation are optimized for successful bone regeneration. The authors discuss advances in different manufacturing techniques including 3D printing and electrospinning that add precision and permeation to scaffold design. Bioactive modifications including growth factor entrapment and surface modification show improvements to osteoconductivity and osteoinductivity enhance scaffold advancement. Lastly, it reviews challenges in clinical translation (e.g., successful vascularization of scaffolds or immune response and healing integration) and future directions (e.g., design with smart or stimuli responsive material properties).

Islam Bouakaz *et al* (2023) says that, This study evaluated the capability of VAT photopolymerization to fabricate hydroxyapatite (HA) scaffolds with a Gyroid TPMS geometry for the advantages in supporting bone repair. The scaffolds were implanted in sheep femurs and after 6 months there were observed no toxic effects to the surrounding tissue; and bone regeneration was achieved. Preliminary evaluations indicate that the HA scaffolds had slightly better early osteointegration and mineralization than the clinical standard, Bio-Oss, but a longer study period (6-12 months) in the sheep is warranted for clinical consideration.

Jiao C *et al* (2022) focusing on mechanical behaviors, bioactivity, and biocompatibility. The authors created porous ceramic scaffolds with biomimetic bone morphology to increase mechanical strength and biological behavior. Using additive manufacturing mechanisms, the authors were able to manufacture scaffolds using porosity and architecture tuned for the scaffold's mechanical requirements, as well as increase cellular attachment and growth with optimized pore geometries. Mechanical

testing demonstrated that the bio-inspired designs had greater strength and toughness than typical scaffolds and were closely matched to the properties of natural bone. The in vitro and in vivo biocompatibility assessments showed that the scaffolds exhibited significant osteoconductivity to support cell proliferation and tissue integration without an adverse immune response. The study presented a demonstration of the use of additive manufacturing to develop patient-specific bone grafts with optimized mechanical and biological properties for clinical use.

Li Y *et al* (2024) says that, This study investigates polymer-ceramic nanocomposite scaffolds for bone tissue engineering and sports injuries. Ceramic nanoparticles enhance mechanical strength, making scaffolds suitable for load-bearing applications. Their biological performance supports cell adhesion and proliferation, essential for bone regeneration. Finite element analysis (FEA) and artificial neural networks (ANN) predict and optimize scaffold performance, demonstrating their potential for regenerative medicine.

Liu Z *et al* (2023) says that, Scaffolds based on TPMS have known superior mechanical properties, and can be improved further to enhance fatigue resistance which is critical for long-term structural performance. This research demonstrated through computational modeling and experimental validation that by modifying the geometric parameters of the scaffold (such as porosity and scale of the unit cell) fatigue life was improved significantly as a result of lowered stress concentrations. The results indicated that application-specific TPMS would be useful to the aerospace, biomedical, and automotive industries where there is a need for structural resilience in cyclic load applications. The study emphasized the opportunity to optimize microstructure in additive manufacturing; in order to produce high-performance materials that are fatigue resistant.

Miaoda Shen *et al* (2023) says that, the results show that both Gyroid and diamond TPMS scaffolds supported osteogenic differentiation and elicited more rapid and consistent uniform bone regeneration than sheet-TPMS geometries. The sheet-TPMS had advantages in mechanical strength and a faster rate of Mg-ion release, which was counter to the much clearer delay in in vivo bone formation resorption with the sheet-TPMS. Overall, the results provide valuable perspective on how much research can progress bioceramic scaffold design and enhance and accelerate osteogenesis for the surgical repair of bone defects.

Perier-Metz C *et al* (2022) says that, Furthermore, the scaffold geometry is important with respect to bone regeneration. Pore size and level of interconnection are important components of engineering a scaffold that promotes good vascularization and bone formation. Bad designs, then, will not provide and satisfactory mechanical support or will not allow for healing or will not allow for complete healing. The study indicates potential for computational modeling to assist with speed and optimization of scaffold development that limits additional expensive, time-consuming *in vivo* studies. *Acta Biomaterialia* is a high-impact, peer-reviewed journal focusing on the evolving field of biomaterials science and publishes current research and developments in materials for medical use. The study falls under the utility of the journal, since it develops biomaterials scaffold designs for the field of regenerative medicine. The study contributes valuable information to the field of tissue engineering and highlights the importance of scaffold microstructure in terms of clinical outcomes in the repair of large bone defects.

Rafieyan S *et al* (2024) says that, machine learning (ML) method to forecast 3D printed scaffold quality for regenerative medicine applications. The authors presented ML models to improve scaffold printing parameters (e.g., mechanical strength, biocompatibility, and/or porosity) and talked about the current issues with repeatability and scaffold performance in this sector. Their machine learning system successfully predicted the slack-constructed output of the scaffold designs using experimental data as input, which finally offered a chance to decrease the amount of trial-and-error involved in the manufacturing of 3D scaffolds. According to the study presented here, scaffold construction may be more easily facilitated by data-driven models. In a broader sense, biofabrication data transformation improves biofabrication process efficiency, accelerating personalized medicine and bioengineering. *Journal biofabrication* has gained prominence (Impact Factor ~6+ in recent years) and has published exceptional examples of research impacting the biofabrication of biomaterials, bioinks, and additive manufacturing. The possible effect of bioprinting technologies on tissue engineering and biomedical engineering could not be ignored. The consensus also contained encouraging provisions for JL's mission of a journal that combined engineering and the biological sciences with viable, scalable biomedical applications. Furthermore, this paper reflects how machine learning (ML) could provide tremendous value in the designing scaffold constructs for 3D printing, which supports the potential for researchers and clinicians to explore patient-specific therapies.

Roldán E *et al* (2024) says that, 3D scaffolds are an improvement over the previous 2D scaffolds in terms of mimicking the complex physiological mechanisms of the natural ligament, and also having better anisotropy, strength, and stress distribution. The finite element analysis showed an increase in load bearing through implementing a 3D scaffold, which is also evident in the experimental studies on the biocompatibility of the 3D scaffolds. Thus, if scaffolds were to be utilised for ligament repairs, the use of the 3D electrospun PVA scaffolds would be beneficial with their superior structure and mechanical properties.

Shen M *et al* (2023) says that, The researchers created 3D-printed bioceramic scaffolds with TPMS structures that represent a native bone architecture and are also optimized for mechanical properties, nutrient transport and cellular adhesion. In vitro and animal studies demonstrated that the scaffolds were osteogenic and enhanced cell proliferation, differentiation, and extracellular matrix deposition. More porous TPMS structures allow for improved vascularization and bone ingrowth compared to other scaffolds. As for TPMS-based bioceramics, the research team accepted the positive implications for bone tissue engineering and suggested a possible alternative for reconstructing critically-sized bone defects.

Shohan S *et al* (2021) says that, The authors sought to improve the quality control for bioprinting processes by addressing structural defects within the scaffold material that did not rely on a destructive examination method. The authors utilized dielectric impedance spectroscopy which measures the electrical properties and has variability with the integrity of the material, and supervised machine learning algorithms to classify the defects identified in the array of findings. *Procedia Manufacturing* is a peer-reviewed journal for conference proceedings that publishes research findings on advancements related to manufacturing technologies. In regard to a venue for innovative research and research in the additive manufacturing field and especially biofabrication, it does not offer the stringent indexing like other journals may require. The research presented identified how sensing technologies and artificial intelligence could potentially be used for the quality assurance processes of additive manufacturing in real time, more importantly, in industries related to biomedically relevant constructs. Further validation could be useful and be recommended in industrial or clinical settings. This paper contributes to the high-impact research agendas tied to smart manufacturing, through an enjoyable article that focused on materials that were independently quantified using non-

destructive test methods relevant to precision industries such as tissue engineering. Furthermore, future work could highlight scalability potential of this work, and lead investigation into integration into in-situ three-dimensional printing

Silvia Ibrahimi *et al* (2024) says that, the scaffolds designed from TPMS were scaffolds with periodic minimal surfaces directing role in the area of bone integration. More than 1000 scaffold designs were created based on TPMS based surfaces. Both linear and non-linear machine learning algorithms were used in order to predict scaffold parameters. These machine learning models were trained to predict mechanical strength, stiffness and porosity based on input parameters from the scaffold design specifications. An automatic feature selection procedure was also used to provide design parameters relative to scaffolds properties.

Wang C *et al* (2021) says that, The researchers fabricated scaffolds with various pore architectures (i.e., cubic, gyroid, and diamond) using selective laser melting (SLM) to determine the influence on bone formation and vascularization. The results indicated the larger, interconnected pores (600–800 μm) scaffold group displayed a greater amount of cell adhesion, proliferation, and osteogenic differentiation vs smaller pores. The mechanical properties and nutrient diffusion improved with gyroid and diamond porosity increased bone ingrowth and blood vessel formation in vivo. The authors concluded that pore geometry and size need to be considered when attempting to optimize both bone regeneration and vascularisation, and that Ti6Al4V scaffolds with tailored designs could improve the functionality of implants with the orthopedic domains.

Wu C *et al* (2023) says that, The authors propose a derivative-aware ML methodology for optimizing lattice structures with respect to mechanical performance and manufacturability. Traditional topology optimization and continuum mechanics approaches can, however, incur considerable computational costs. Nonetheless, when using ML, this methodology, produces optimal designs while reducing the computational costs needed for the process. The focus is on an optimization process that considers the gradients of behaviors while implementing ML algorithms to help optimize lattice unit cells under load to meet distance constraints to ensure integrity of structural performance under load. Their approach permits gradual transitions in the material gradient as well as improving stress distribution and weight reduction. Validations were made through

simulations and experimental validations for both lattices demonstrated performance improvements beyond classical methodologies. Contributions include a framework for optimizing FGLS with less effort and in improvements to accuracy while enabling simple designs for the complex applications of AM. The outcomes of their research emphasized the ability of ML to advance AM designs, especially for complex Applications such as aerospace, biomedical, and automotive applications, where lightweight and high-strength is important. Overall, the authors indicated research that was comprehensive and described the relationship and interaction between ML and AM for more intelligent ways of manufacturing.

Yao D *et al* (2023) says that, the use of parametric modeling and selective laser sintering (SLS) to develop gradient scaffolds, or scaffolds with mechanical properties and porosity that vary, for bone tissue engineering and other applications. The authors computationally modeled scaffold architectures to optimize the design of scaffolds with controlled stiffness and axial strength gradients, created the gradient scaffolds using SLS, and conducted mechanical testing of the scaffolds. They demonstrated that gradient scaffold designs performed better than scaffolds with uniform structures with respect to the measures of the mechanical testing and provided better load distribution and energy absorption. The authors suggested that parametric modeling can be used to generate scaffolds and customize scaffolds for biomedical and industrial applications, and also created also variably functional structure through variation of material property.

Yongyue Li *et al* (2024) says that, This study developed biomimetic Ti6Al4V scaffolds to replicate the natural gradients seen in bone using Electron Beam Melting (EBM). The gradient designs enhance mechanical strength, integration with bone, and proliferation of cells while closely mimicking bone properties. The results are promising in suggesting this type of scaffold may be a solution to orthopaedic implants with increased stability and osseointegration for clinical purposes.

Yu T *et al* (2024) says that the use of extracellular vesicle (EV)-functionalized bioactive scaffolds for bone regeneration. Extracellular vesicles (EVs) are nanoscale particles secreted by cells and involved in cell communication and tissue repair. The researchers created bioactive scaffolds that are coated with EVs to accelerate bone healing by promoting osteogenesis (bone formation) and angiogenesis (blood vessel formation). The results demonstrated that EV-coated scaffolds significantly improved bone

regeneration when grafted on bone defects when compared to scaffolds without EVs, highlighting a novel advancement in the reconstruction of bone conditions. This study presents EV-coated scaffolds as a strategy for repairing bone defects and demonstrates the use of EVs combined with biomaterials for bioengineering complex therapeutic strategies in tissue engineering.

Yuting Lv *et al* (2022) says that, The proposed project aims to investigate optimized Nickel-Titanium-Niobium (Ni-Ti-Nb) alloys for biomedical application, such as bone implants. Alloy structures will be assembled into scaffolds in Triply Periodic Minimal Surfaces (TPMS) with controlled gradient porosity using the scaffolds to create an effective balance between mechanical properties and bio-functioning scaffolds. The scaffolds will be produced by Selective Laser Melting (SLM). SLM is the newest additive manufacturing (3D printing) technology that allows construction of microstructure and porosity distribution with precision. Once manufactured, the mechanical properties of the scaffolds will be tested to determine their strength, life, and load-bearing capability. The in-vitro biocompatibility of the scaffolds will also be determined using cell attachment, proliferation and biological response measurements; if validated as an applicable scaffold on preliminary testing, the scaffolds could go forwards to preclinical testing as bone implants.

Zihang Wang *et al* (2022) says that, the overall project aim is to minimize stiffness in Ti6Al4V orthopedic implants to reduce stress shielding through 3D-printed porous titanium alloy scaffolds to simulate trabecular structure with adjustable pore sizes (300/400/500 μm). The early results demonstrate the scaffolds to support cell proliferation and osseointegration, profuse at pore size 400 μm .

2.3 INFERENCE FROM LITERATURE REVIEW:

Pore Size and Porosity:

Research highlights the critical role of scaffold porosity in bone regeneration. Optimal pore sizes, typically ranging from 50 to 400 μm , facilitate cell infiltration, vascularization, and tissue growth, ensuring effective bone healing.

Finite Element Analysis (FEA):

FEA is widely utilized for mechanical testing of scaffolds, providing insights into stress distribution and structural integrity. However, only a limited number of studies incorporate machine learning (ML) for scaffold optimization, presenting an opportunity for further advancements in this area.

Material Selection:

Commonly used scaffold materials include polymers such as polylactic acid (PLA) and polycaprolactone (PCL), ceramics like hydroxyapatite (HA) and β -tricalcium phosphate (β -TCP), and metals such as Ti6Al4V. Composite materials are particularly advantageous as they combine mechanical strength with bioactivity, making them well-suited for bone tissue engineering.

Potential of Machine Learning (ML):

While some studies have applied ML for predicting scaffold performance, full automation of scaffold optimization remains largely unexplored. This gap highlights the potential for integrating ML techniques to streamline scaffold design and improve efficiency in regenerative medicine.

CHAPTER 3

PROBLEM DESCRIPTION

3.1 BONE DEFECT AND BONE LOSS:

Bone defect and bone loss pose major problems in orthopedic and reconstructive medicine. These issues often stem from trauma, disease, or conditions present at birth. The image shows a cutting-edge way to fix these problems starting with spotting bone defects. Next, experts make a custom scaffold plan to fit the exact shape of the defect. They build this design through Fused Deposition Modeling (FDM), a 3D printing method that gives them full control over the scaffold's pores and structure. The printed scaffold then goes through tissue culture where cells are added and it's prepared to help tissue grow back. In the final step, doctors put the engineered scaffold into the body. This scaffold helps new bone to form and brings back the strength and use of the damaged bone area. This process shows how advanced design, manufacturing, and biological methods work together to treat bone loss well.

3.2 PROBLEM STATEMENT:

The goal of this project is to optimize and automate the design and material selection process for personalized bone scaffolds, ensuring they meet specific strength and porosity requirements. By leveraging advanced computational analysis and machine learning techniques, the system aims to generate customized scaffold structures tailored to individual patient needs. A key challenge in this process is addressing the issue of low strength, which must be improved while maintaining the necessary porosity for proper cell growth and integration. The ultimate objective is to enhance the performance and reliability of bone scaffolds, leading to better patient outcomes in regenerative medicine and orthopedic applications.

3.3 OBJECTIVE:

The primary objectives of this project are to optimize and automate the design process of bone scaffolds to ensure they meet customized strength and porosity requirements while maintaining structural integrity. By leveraging advanced computational techniques, the project aims to streamline scaffold generation, reducing manual

intervention and improving efficiency. Additionally, it focuses on enabling patient-specific customization, allowing scaffold designs to be tailored to individual anatomical structures and functional needs. This personalization ensures better compatibility, enhanced biomechanical performance, and improved integration with natural bone tissue. Addressing these goals, the project is driven by the problem statement: “To optimize and automate personalized Bone Scaffold Design and Material that meets specific strength and porosity requirements.

CHAPTER 4

METHODOLOGY

4.1 WORKFLOW METHODOLOGY OF THE PROJECT:

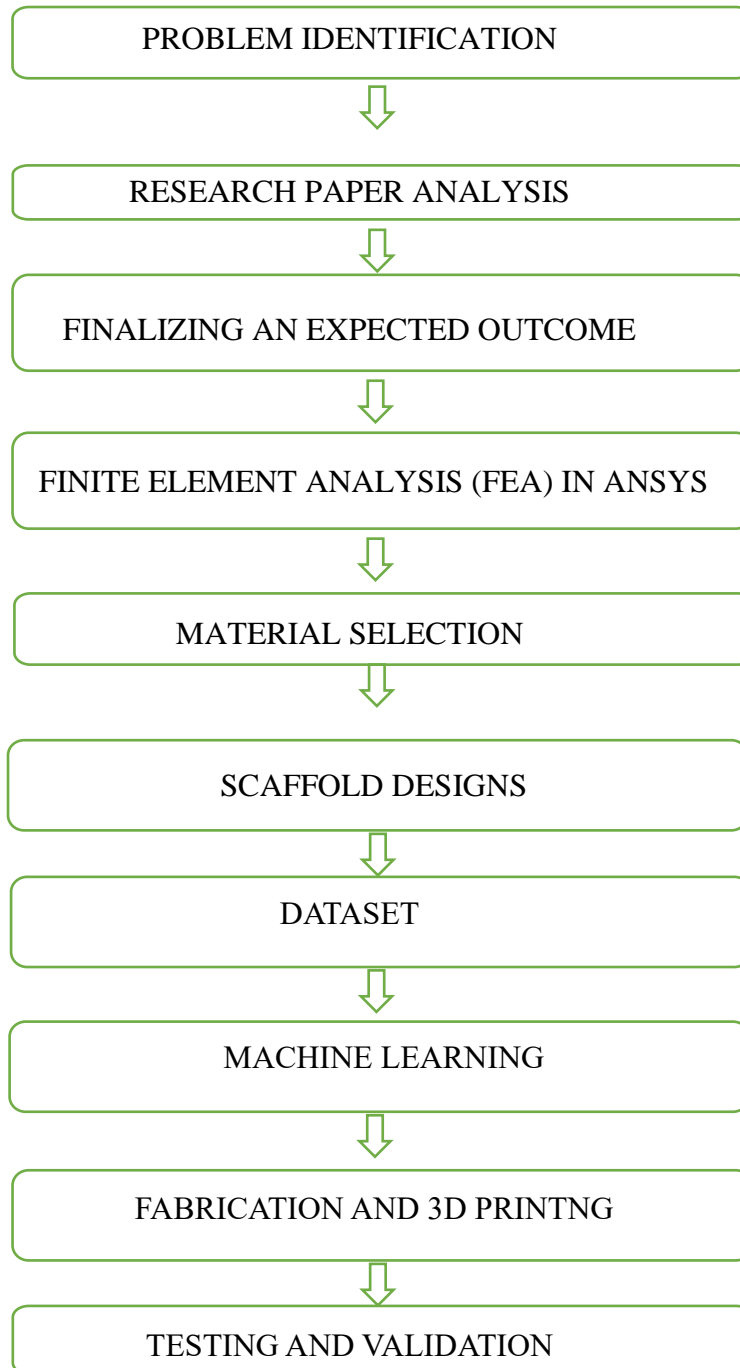


Figure 4.1 Workflow of project

The above figure 4.1 represents the sequence of processes involved in the entire project. Initially the bone structure and defects were studied and then the influence of biomaterials

in bone tissue engineering was studied. The market survey for bone defects and biomaterials was taken. The literature review was done and the problem definition and objective were derived. And then the materials and methods for bone tissue engineering was poly lactic acid based biopolymer and FDM 3D printing respectively. The filament for FDM 3D printing was bought and the scaffolds were designed and fabricated. The tests were carried out on the scaffolds and finally the results were interpreted.

CHAPTER 5

EXPERIMENTAL SET-UP

5.1 SCAFFOLD DESIGN AND GENERATIONS:

In this project, scaffold structures are created by placing small pores inside a cube. These pores must be evenly spaced and should not overlap, while still keeping enough wall thickness for strength. Doing this manually is slow and often leads to mistakes in spacing or alignment.

In scaffold structure automation, input parameters play a very important role. They decide how the final structure will look and perform. Without setting clear parameters, it would not be possible to create accurate and reliable scaffolds automatically.

5.1.1 PARAMETERS:

parameter were used for create a structure with not hole interest each other and to avoid to much spaces also avoided based on input thickness and pore diameter to calculated to structure is created and based on below formulas

5.1.2 AVAILABLE LENGTH FOR HOLES:

$$A_x = L_x - 2t_{\text{outer}} \quad \dots(5.1)$$

$$A_y = L_y - 2t_{\text{outer}} \quad \dots(5.2)$$

$$A_z = L_z - 2t_{\text{outer}} \quad \dots(5.3)$$

The Formulas **5.1,5.2,5.3** used to identify the available spaces for pores created after margin this subtracted

5.1.3 SPACING BETWEEN PORES:

$$S_x = \frac{A_x - N_x \cdot D_p + D_p}{N_x - 1} \quad \dots(5.4)$$

$$S_y = \frac{A_y - N_y \cdot D_p + D_p}{N_y - 1} \quad \dots(5.5)$$

$$S_z = \frac{A_z - N_z \cdot D_p + D_p}{N_z - 1} \quad \dots(5.6)$$

The Formulas 5.4,5.5,5.6 to calculated the spaces between pores per each axis

5.1.4 WALL THICKNESS CHECK:

$$t_{\text{wall},x} = S_x - D_p \geq t_{\min} \quad \dots(5.7)$$

$$t_{\text{wall},y} = S_y - D_p \geq t_{\min} \quad \dots(5.8)$$

$$t_{\text{wall},z} = S_z - D_p \geq t_{\min} \quad \dots(5.9)$$

The Formulas **5.7,5.8,5.9** to check the minimum thickness condition is satisfy or not.

5.1.5 RECOMMENDED NUMBER OF HOLES:

$$N_x = \left\lceil \frac{L_x - 2t_{\text{outer}} + t_{\min}}{D_p + t_{\min}} \right\rceil \quad \dots(5.10)$$

$$N_y = \left\lceil \frac{L_y - 2t_{\text{outer}} + t_{\min}}{D_p + t_{\min}} \right\rceil \quad \dots(5.11)$$

$$N_z = \left\lceil \frac{L_z - 2t_{\text{outer}} + t_{\min}}{D_p + t_{\min}} \right\rceil \quad \dots(5.12)$$

The Formulas **5.10,5.11,5.12** to calculate a number of pores per axis based cube, pore diameter, minimum thickness

5.1.6 HOLE CENTRE POSITIONS:

$$P_{i,x} = -\frac{L_x}{2} + t_{\text{outer}} + \frac{D_p}{2} + i \cdot S_x \quad \text{for } i = 0, 1, \dots, N_x - 1 \quad \dots(5.13)$$

$$P_{j,y} = -\frac{L_y}{2} + t_{\text{outer}} + \frac{D_p}{2} + j \cdot S_y \quad \text{for } j = 0, 1, \dots, N_y - 1 \quad \dots(5.14)$$

$$P_{k,z} = -\frac{L_z}{2} + t_{\text{outer}} + \frac{D_p}{2} + k \cdot S_z \quad \text{for } k = 0, 1, \dots, N_z - 1 \quad \dots(5.15)$$

The formulas are 5.13,5.14,5.15 calculated the pore positions based on cube, pore diameter, spacing and the number of pores to vary the i, j, k as per number of pores in axis

5.2 PORE SHAPES:

The selected pore shapes for scaffolds are Square, Circle, Hexagon, Pentagon, Diamond.

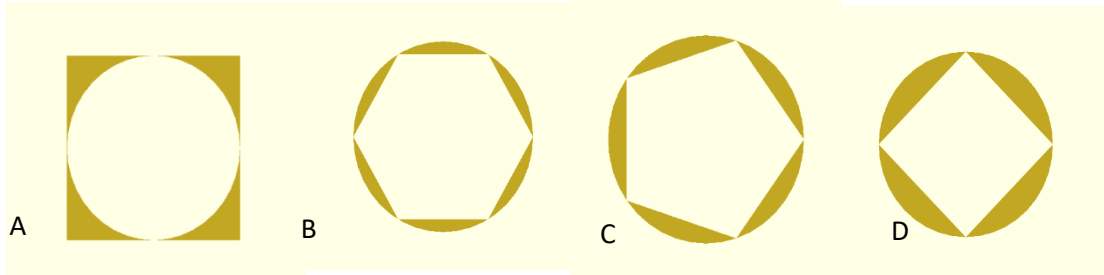


Figure 5.1 A) Square and Circle B) Circle and Hexagon C) Circle and Pentagon
4) Circle and Diamond

5.2.1 PORE AREA

The all shapes maintain the pore diameter based on this formulas 5.16,5.17,5.18,5.19,5.20 to find the pore areas for shapes shown in figure 5.1 A) Square And Circle B) Circle And Hexagon C) Circle And Pentagon 4) Circle And Diamond.

SQUARE AREA: $A_{\text{square}} = s^2$ (5.16)

CIRCLE AREA: $A_{\text{circle}} = \pi \left(\frac{d}{2}\right)^2 = \frac{\pi d^2}{4}$ (5.17)

HEXAGON AREA: $A_{\text{hexagon}} = \frac{3\sqrt{3}}{2} \left(\frac{d}{2}\right)^2 = \frac{3\sqrt{3}d^2}{8}$ (5.18)

PENTAGONAL PORE AREA: $A_{\text{pentagon}} = 0.59441 \times s^2$ (5.19)

DIAMOND PORE AREA: $A_{\text{diamond}} = 0.5 \times d^2$ (5.20)

5.3 STRCUTURE CREATIONS:

The regular pore structure were created using a software contains a function of structure with Boolean operations and a parameters to control a structure.

5.3.1 OPENS CAD STRCUTURE CREATIONS:

OpenSCAD is a free and open-source software designed for creating 3D models through programming. It is especially suitable for applications that require high customization and repetitive geometric patterns, such as scaffold structures. The modeling process typically begins with generating a cube using the `cube([x, y, z], center = true)` command, which centers the cube at the origin. To introduce porosity, vertical cylinders are created using the `cylinder(h, d)` function. These cylinders, representing pores, are arranged in a regular grid by applying for loops, and positioned accurately with the `translate([x, y, z])` command. The `difference()` function is then employed to subtract all the cylinders from the cube, leaving behind a perforated structure. This scripting-based method is highly automatable, accurate, and well-suited for scientific and biomedical designs like porous scaffolds. The final model can be exported in STL format for further processing or 3D printing.

5.3.2 CADQUERY STRCTURE CREATIONS:

Initially, OpenSCAD was chosen to design the scaffold structure due to its simplicity and precise control through code. Its scripting-based approach made it easy to generate repetitive patterns like pores. However, as the design complexity increased, OpenSCAD became less efficient. Since it processes tasks using only a single CPU core, it struggled to handle larger models, leading to longer rendering times.

To overcome this limitation, the workflow shifted to CadQuery, a Python-based modeling library. CadQuery is better suited for complex geometries and performs faster, especially for large or intricate structures. Its integration with Python also enables seamless automation and easy manipulation of design parameters, such as the number and size of holes, without needing to rebuild the model from scratch.

In CadQuery, the scaffold is built using intuitive Python commands. A solid base is created using the `box()` function, and cylindrical holes are added with `cylinder()`. These holes are positioned accurately using loops and `translate()`, then subtracted from the block using `cut()` to form the porous structure. CadQuery's flexibility allows for quick updates to the model and supports direct export to STL and STEP formats, which are widely used

for 3D printing and simulation. This makes it an efficient and scalable tool for advanced scaffold design.

5.3.3 STRUCTURE AUTOMATION:

The structure were created based on the inputs as Cube sizes, number of pores, pore shape, pore diameter. The python code is used to get the start, stop, step values as required parameter then calculated the parameters list contains values and recommended holes is a Boolean function is true the number of holes calculated based on inputs rather than manual number of holes for improving the structure creation without any errors. The inputs parameters to created a unique name and stl file path were saved in dataset. It contains input parameters such as cube, number of pores, thickness, margin, pore shape, pore diameter, pore area, stl file name and path.

	Start	Stop	Step
Cube Width	12.7		
Cube Breadth	12.7		
Cube Height	12.7		
Num Holes Width			
Num Holes Breadth			
Num Holes Height			
Shape	1	6	1
Pore Dia	0.2	1.2	0.2
Min Thickness	1		
Set Margin	0.5		

☒ Recommended Num Holes
 ☐ Num Holes H In

Submit

Figure 5.2 The Tkinter interface for a structure automation

The python sub process run call a openscad to create a structure, for a cadquery is used python cadquery package to created python environment so no other software required. From the figure 5.2 To input parameters cube prism dimensions are 12.7,12.7,25.4 mm, pore diameter vary 0.2 to 1 as step 0.2, minimum thickness set as 1mm, set margin in an outer edge set 0.5 and the shapes vary 1 to 5 with step 1 so the

total combinations file get 25 files and check conditions to create and save as STL file format.

5.4 POROSITY CALCULATION:

5.4.1 POROSITY:

Porosity is an essential metric for evaluating scaffold structures, as it quantifies the void spaces in relation to the total volume of the structure. The **formula 5.21** used to calculate the porosity

$$\text{Porosity}(\%) = \left(1 - \frac{V_{\text{solid}}}{V_{\text{bounding box}}}\right) \times 100 \quad \dots(5.21)$$

Where,

V_{solid} is the **actual solid volume** of the 3D scaffold.

$V_{\text{bounding box}}$ is represents the **volume of the smallest box** that fully encloses the model.

5.4.2 SOLID VOLUME

The solid volume of the 3D model is calculated using the `get_mass_properties()[0]` function from the `numpy-stl` library. This function estimates volume by summing the contributions of all triangle-based facets that form the mesh, using the formula 5.22

$$V_{\text{triangle}} = \frac{1}{6} \times |v_1 \cdot (v_2 \times v_3)| \quad \dots(5.22)$$

where $\vec{v}_1, \vec{v}_2, \vec{v}_3$ are the vertices of each triangular face.

5.4.3 TOTAL VOLUME

The total volume of the object is represented by the bounding box volume, which is the space occupied by the smallest rectangular box that can enclose the entire model. This is calculated by multiplying the length, width, and height of the bounding box. The formula 5.24 to calculate bounding box volume.

$$V_{\text{bounding box}} = \text{Length} \times \text{Width} \times \text{Height} \quad \dots(5.23)$$

5.4.4 SURFACE AREA

The surface area of the model is calculated by summing the areas of all its triangular faces. The area of each triangle is determined by the cross product of two vectors formed by the triangle's vertices. This approach adds up the areas of all the individual triangles to give the total surface area of the model. The formula 5.25 is used to calculate the area of a triangle.

$$A_{\text{triangle}} = \frac{1}{2} \times |(v_2 - v_1) \times (v_3 - v_1)| \quad \dots(5.24)$$

where $\vec{v}_1, \vec{v}_2, \vec{v}_3$ are the vertices of each triangular face.

5.4.5 POROSITY AUTOMATION:

The Python code works by reading STL file paths from a dataset and using **Trimesh** and **numpy-stl** libraries to gather important geometric details from each 3D model. For every STL file, the model is loaded, and key properties like **solid volume**, **bounding box volume**, and **surface area** are calculated with functions from **Trimesh**. These results are then saved into a new CSV file, making it easy to access and analyze the data for future use. The figure 5.3 shows the tkinter GUI for porosity calculation based on dataset, folder, stl file for a simple GUI-based workflow.

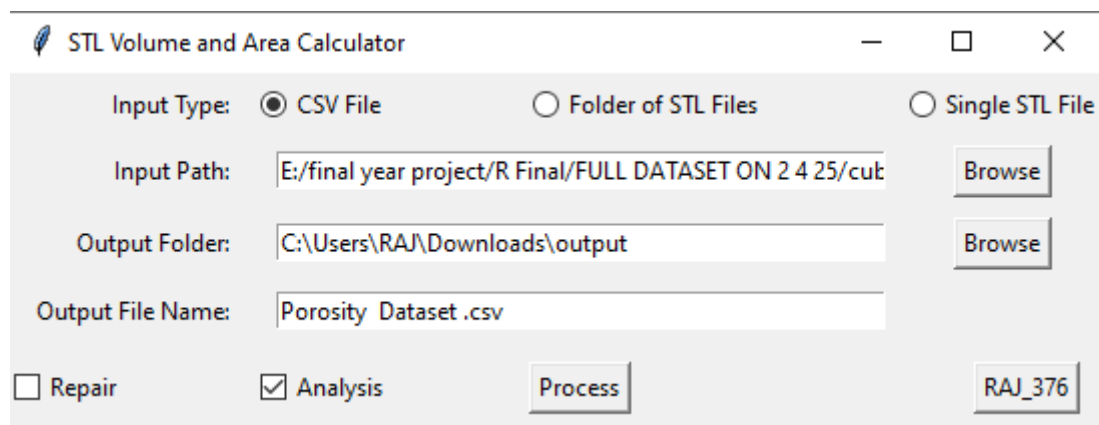


Figure 5.3 The tkinter GUI for porosity calculation based on dataset, folder, stl file

5.5 DESIGN OF SCAFFOLD

5.5.1 SQUARE PORE SCAFFOLD:

A cube sized scaffold of 12.7mm x 12.7mm x 25.4mm were designed with square pores of sizes 1mm. The front view, side view and top view of the square pore scaffolds were shown below in the **figure 5.4**.

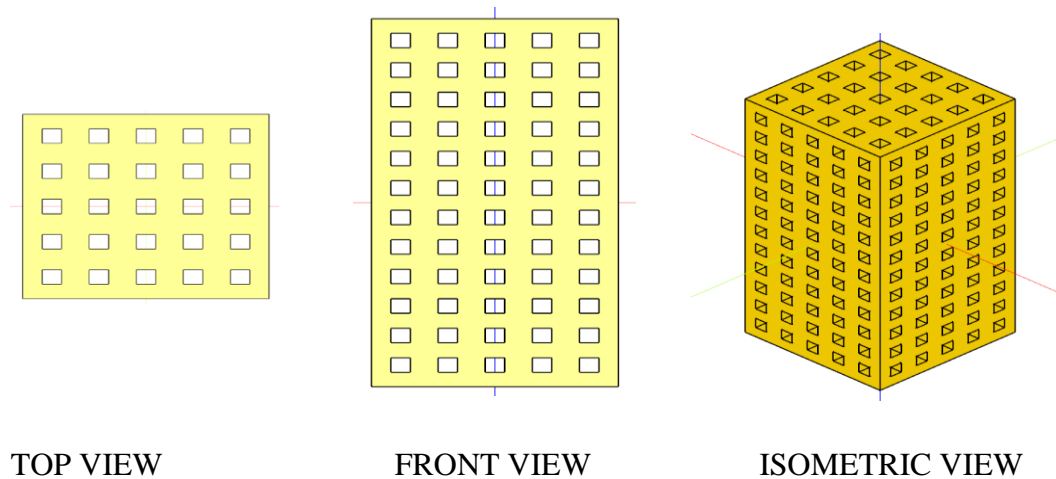


Figure 5.4 Square pore scaffold with 1mm pore size

5.5.2 CIRCLE PORE SCAFFOLD:

A cube sized scaffold of 12.7mm x 12.7mm x 25.4mm were designed with circle pores of sizes 1mm. The front view, side view and top view of the circle pore scaffolds were shown below in the **figures 5.5**.

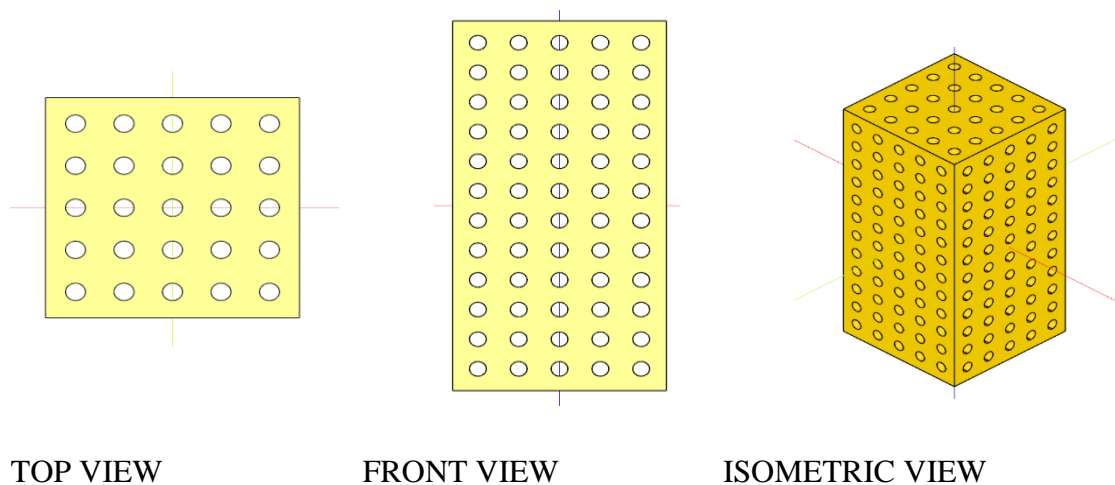


Figure 5.5 Circle pore scaffold with 1mm pore size

5.5.3 HEXAGON PORE SCAFFOLD:

A cube sized scaffold of 12.7mm x 12.7mm x 25.4mm were designed with hexagon pores of sizes 1mm. The front view, side view and top view of the hexagon pore scaffolds were shown below in the **figure 5.6**.

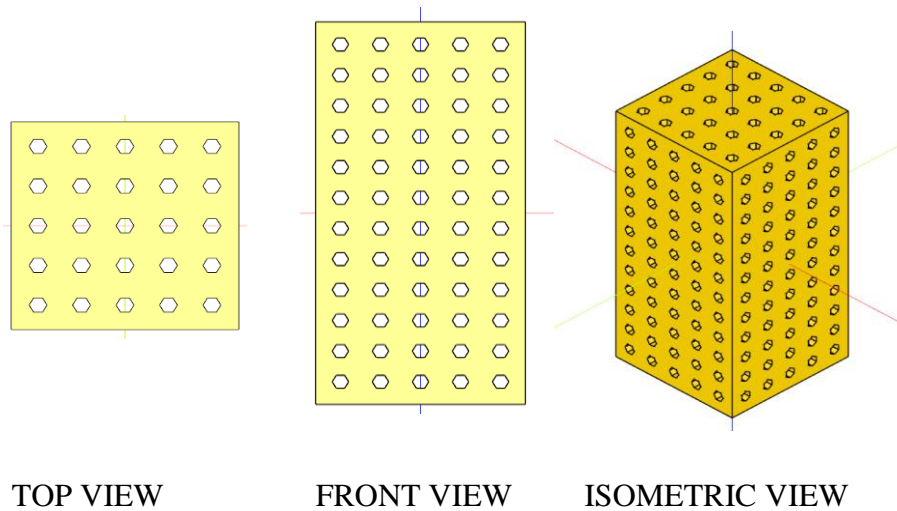


Figure 5.6 Hexagon pore scaffold with 1mm pore size

5.5.4 PENTAGON PORE SCAFFOLD:

A cube sized scaffold of 12.7mm x 12.7mm x 25.4mm were designed with pentagon pores of sizes 1mm. The front view, side view and top view of the pentagon pore scaffolds were shown below in the **figure 5.7**.

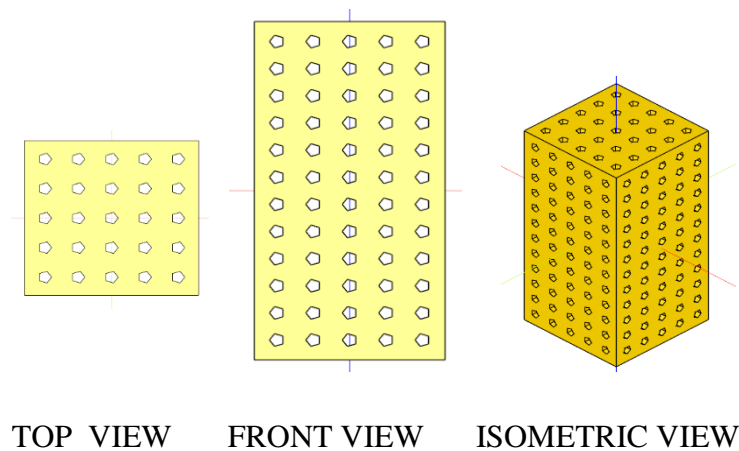


Figure 5.7 Pentagon pore scaffold with 1mm pore size

5.5.5 DIAMOND PORE SCAFFOLD:

A cube sized scaffold of 12.7mm x 12.7mm x 25.4mm were designed with diamond pores of sizes 1mm. The front view, side view and top view of the diamond pore scaffolds were shown below in the **figure 5.8**

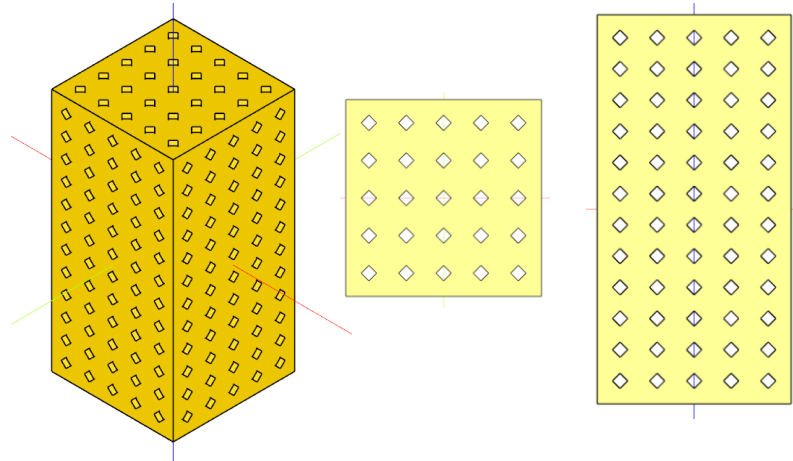


Figure 5.8 Diamond pore scaffold with 1mm pore size

5.6 FABRICATION OF SCAFFOLD:

5.6.1 FABRICATION OF SCAFFOLDS BY FDM

Commercially available Poly Lactic Acid (PLA) filament with a diameter of 1.75 mm was used for scaffold fabrication. Additionally, PLA–Graphene filament was directly fed into the FDM printer. The printer was equipped with a 0.4 mm nozzle. Printing parameters were set as follows: a speed of 40 mm/s, a layer thickness of 0.2 mm, and an infill density of 100%. The nozzle and build plate temperatures were maintained at 200 °C and 60 °C, respectively. Scaffold fabrication was carried out using these parameters. The FDM printer used was an ENDER 3 model, offering a build volume of 220 mm × 220 mm × 250 mm.

5.6.2 SQUARE, CIRCULAR, HEXAGONAL, DIAMOND AND PENTAGON PORE SCAFFOLD:

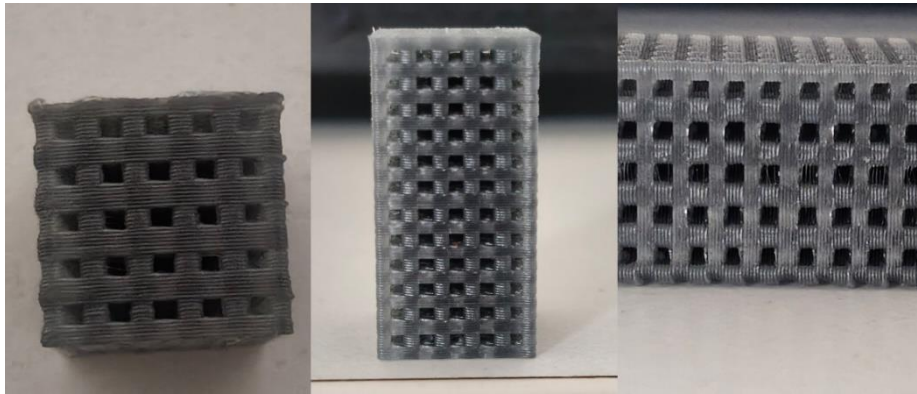


Figure 5.9 Square pore scaffold with pore size 1mm

The scaffolds were fabricated using the above ENDER 3 FDM machine and the fabricated square pore scaffold (pore sizes 1mm), circular pore scaffold (pore sizes 1mm), hexagonal pore scaffold (pore sizes 1mm), Diamond pore scaffold (pore sizes 1mm), Pentagon pore scaffold (pore sizes 1mm) were shown in the **figure 5.9, 5.10, 5.11, 5.12 and 5.13** respectively.

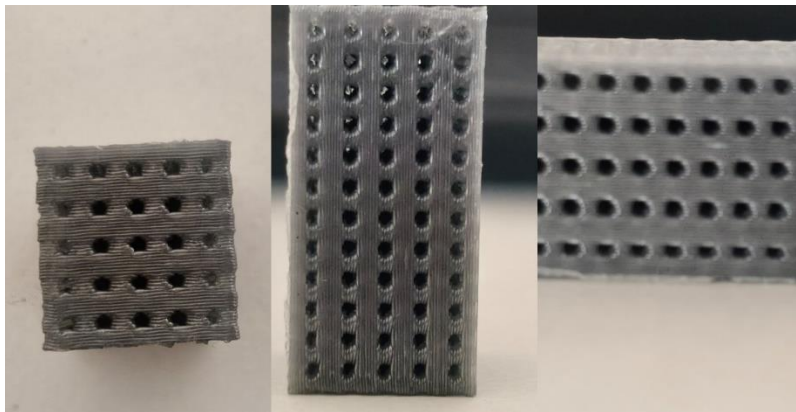


Figure 5.10 Circle pore scaffold with pore size 1mm

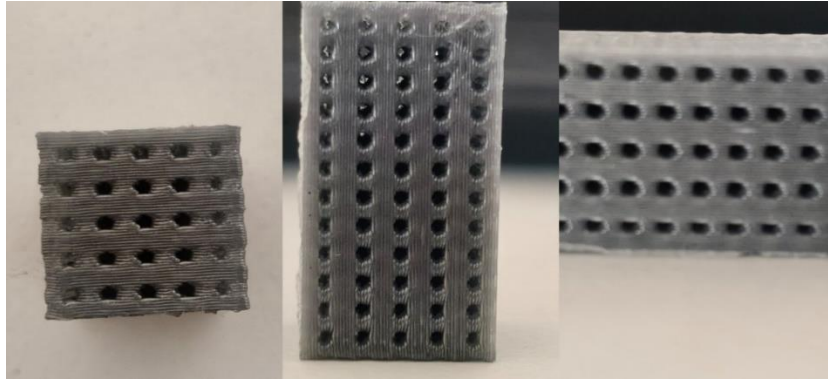


Figure 5.11 Hexagonal pore scaffold with pore size 1mm

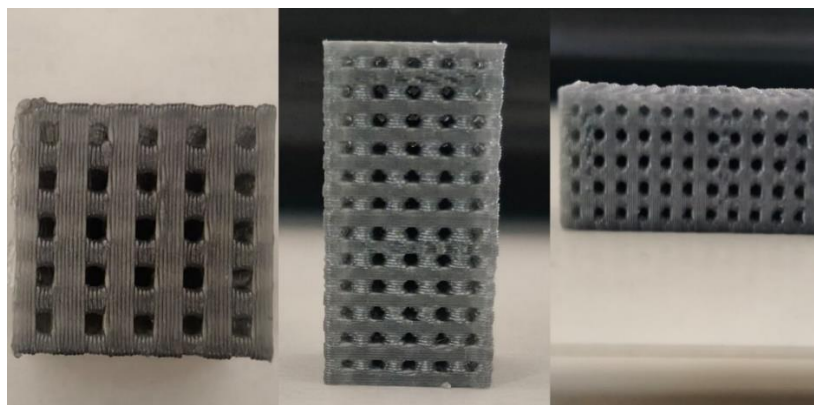


Figure 5.12 Diamond pore scaffold with pore size 1mm

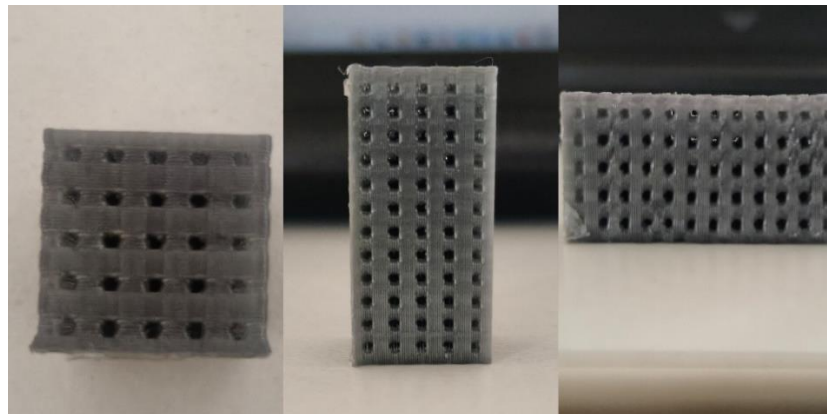


Figure 5.13 Pentagon pore scaffold with pore size 1mm

5.7 FEA ANALYSIS

5.7.1 File conversion

To understand how the scaffold structures behave under mechanical loading, finite element analysis (FEA) was performed. The 3D models of these irregular porous scaffolds were initially designed in STL format, which is not directly suitable for simulation. Therefore, each STL file was converted into a STEP file—a standardized format better suited for CAD and simulation software. This conversion process was carried out using ANSYS SpaceClaim, where the models were refined by merging surfaces and ensuring the geometry formed a valid solid body. To handle multiple files efficiently, an IronPython script was implemented. This script reads a dataset containing the paths to the STL files, automates the import and cleanup within SpaceClaim, and exports each model as a STEP file. This automated workflow significantly speeds up the pre-processing stage and enables batch simulations of various scaffold designs in ANSYS Workbench.

5.7.2 Ansys Simulations

To streamline the simulation process in ANSYS Workbench, we developed an automated Python-based workflow. This script was designed to import the mechanical properties of PLA material and assign it to the solid model as the designated material for analysis. The geometry files, whose paths were provided in a structured dataset, were automatically imported into the Workbench environment. To optimize simulation time and reduce computational demands, a default mesh configuration was used, which offers a good balance between accuracy and processing efficiency for complex scaffold geometries.

In addition, the automation setup included the use of named selections to identify the top and bottom surfaces of the scaffold in the Z-direction. This allowed for precise and repeatable application of boundary conditions. A compressive load of 2000 N was applied to the top surface using these named selections, while the bottom surface was fixed to simulate a realistic compression test scenario. This automated setup not only improved simulation consistency but also significantly reduced manual effort in preparing multiple scaffold models for analysis.

5.8 MACHINE LEARNING APPROACH

A diverse dataset was developed by systematically varying key structural parameters of scaffold cubes, including their width, breadth, height, pore diameter, pore shape (numerically encoded), and the number of holes aligned along each principal axis. Based on these core geometric features, secondary characteristics such as wall thickness, porosity, and permeability were calculated using computational methods. The final dataset consisted of 2300 unique scaffold configurations. However, due to the intensive computational resources required for finite element analysis (FEA), mechanical simulations were performed on a subset of 108 representative models. These were carefully chosen to reflect a broad range of pore sizes, shapes, and hole distributions, ensuring the mechanical analysis provided meaningful insights across the design space.

In this project, a comprehensive machine learning workflow was developed to accurately predict both structural and mechanical characteristics of porous scaffolds derived from parametric cube designs. The original dataset contained 2300 samples, each defined by key geometrical and pore-related parameters such as cube size (length, width, and height), the number of pores along each principal axis, pore diameter, shape type (numerically encoded), and margin spacing between pores. After eliminating duplicate entries and applying outlier detection using the Z-score method (threshold $|Z| > 3$), a refined dataset of 2049 samples was prepared for modeling. This data was split into training (70%), validation (15%), and testing (15%) sets to ensure balanced and unbiased model evaluation. Feature standardization was carried out using the StandardScaler from scikit-learn to normalize input distributions. The study focused on four key regression tasks: (i) predicting porosity using full geometric input, (ii) estimating permeability based on cube and pore parameters, (iii) determining pore counts in all three directions from porosity and overall dimensions, and (iv) forecasting mechanical outcomes such as equivalent stress, equivalent strain, maximum deformation, and maximum principal stress. A suite of regression models—Linear Regression, Ridge, Lasso, Random Forest, Gradient Boosting, Support Vector Regression (SVR), and XGBoost—were trained and compared based on standard evaluation metrics, including R^2 , Mean Absolute Error (MAE), and Root Mean Squared Error (RMSE). The best-performing models were saved using joblib and later used for unseen test data and real-time prediction. Model performance and behavior were analyzed through visualization tools such as prediction

plots, residual diagnostics, and feature importance graphs. This pipeline supports efficient scaffold design and optimization through data-driven methods, in line with current trends in AI-assisted materials engineering and biomedical design.

5.9 EXPERIMENTAL SETUP:

5.9.1 ARCHIMEDES POROSITY MEASUREMENT

The porosity of the scaffold is measured using the Archimedes porosity determination by liquid saturation method. A cube shaped scaffold were made for each pore shape and size of the scaffold. The porosity of the scaffold for all the scaffolds with each pore shape and size was calculated and the average porosity percentage of the scaffolds was calculated for overall porosity determination. Porosity is determined using the formula 5.25

$$\text{Porosity}_{\text{actual}}(\%) = \left(\frac{\Delta W}{\rho_{\text{ethanol}} \times V_{\text{total}}} \right) \times 100 \quad \dots(5.25)$$

Where

$\Delta W = W_{\text{wet}} - W_{\text{dry}}$ (g) - The difference in weight before and after immersion in ethanol. $\rho_{\text{ethanol}} = 0.789 \text{ g/cm}^3$ - The density of ethanol at room temperature. $V_{\text{total}} = 4.1031 \text{ cm}^3$ - The total volume of the scaffold ($12.7 \times 12.7 \times 25.4 \text{ mm}^3$). The experimental setup is shown in figure 5.14



Figure 5.14 Porosity measurement setup

5.9.2 COMPRESSION TEST:

MECHANICAL TESTING:

To assess the structural stability and mechanical properties of the constructed scaffold, a uniaxial compression test was performed. The scaffold, measuring $12.7\text{ mm} \times 12.7\text{ mm} \times 25.4\text{ mm}$, was compressed under a compressive force using a Universal Testing Machine (UTM). The procedure was determined as per ASTM D1621 and ASTM D695 standard. The sample was placed vertically in between two flat platens of compression, and the load was applied at a constant rate per time (1mm/min). Force and displacement were measured during the test to get stress-strain curves. Important parameters like compressive strength, Young's modulus, and deformation behavior were measured. This test is necessary for evaluating the load-carrying capacity of the scaffold and determining its failure modes under mechanical loading, which is very important for structural and biomedical engineering applications.



**Figure 5.15 BISS Nano Test System
BI-7000 Machine**

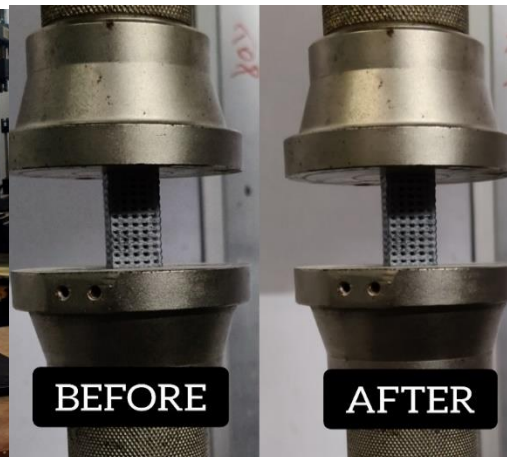


**Figure 5.16 Before and After
Compression Testing**

5.9.3 PERMEABILITY ANALYSIS

Understanding fluid flow through scaffolds is a critical aspect of tissue engineering, as it directly influences cell viability, nutrient delivery, and waste removal. In this study, the permeability of 3D-printed PLA scaffolds is estimated using the Kozeny–Carman equation, a well-established theoretical model. This equation links permeability to two important structural properties of the scaffold—porosity and the specific surface area per unit volume—enabling predictions of fluid transport based purely on the scaffold’s geometry. The formula 5.28 to calculate the permeability using constanst as 5 for pla.

One of the key benefits of this approach is that it provides a quick and reliable way to estimate permeability without requiring complex and time-intensive experimental procedures. This makes it especially useful in the early design phase, where multiple scaffold variations are being evaluated. While the Kozeny–Carman equation was initially developed for idealized porous materials, it has been successfully adapted for use in biomaterial research. In this work, the focus is on estimating scaffold permeability based solely on porosity, providing valuable insights into fluid behavior across different scaffold designs.

$$k = \frac{\phi^3}{(1-\phi)^2 \cdot c \cdot s^2} \quad \dots(5.26)$$

Where,

k = permeability

ϕ = porosity

c = Kozeny constant

s= specific surface area per unit volume

CHAPTER 6

RESULTS AND DISCUSSION

6.1 FEA RESULTS:

The FEA software ANSYS workbench and iron python code use to automatically import geometry, applied loads and condition to export the results to csv. In this project we choose a default mesh for all analysis in static condition for reduce computational power. **Figure 6.1** A) Mesh set as a default mesh B) Equivalent Stress for check the structure whether is under the yield reign for avoid yield failure C) Equivalent Strain for identity elastic strain D) Maximum Principal Stress for a stress under tensile strength is exits the tensile strength structure become crack or failure E) Total Deformation is identify the stiffness of the structure F) Normal Stress for a axial stress along the axis for applying a load.

The cube prism 12.7 mm, 12.7 mm ,25.4 mm cube was created 5*5*12 holes on pore dia 1 and the shape varies from square, circle, hexagon, pentagon, diamond applied a 2000N load on pla got a mechanical result as Table 6.1.

Table 6.1 FEA results for pore diameter 1mm

Shape name	Equ._ stress (pa)	Equ._ Strain (m/m)	Normal _ z (pa)	Max._ principal (pa)	Max._ Deformation(m)	Porosity (%)
SQUARE	53295.74	1.56E-05	-73294.1	-23113.3	7.92E-06	38.05
CIRCLE	113565	3.25E-05	-142296	-31800.3	6.88E-06	30.89
HEXAGON	100324	2.97E-05	-117837	-19050.3	6.27E-06	26.46
PENTAGON	96635.29	2.83E-05	-110582	-20631.8	6.04E-06	24.52
DIAMOND	54713.49	1.93E-05	-78405.9	-27322.4	5.63E-06	20.85

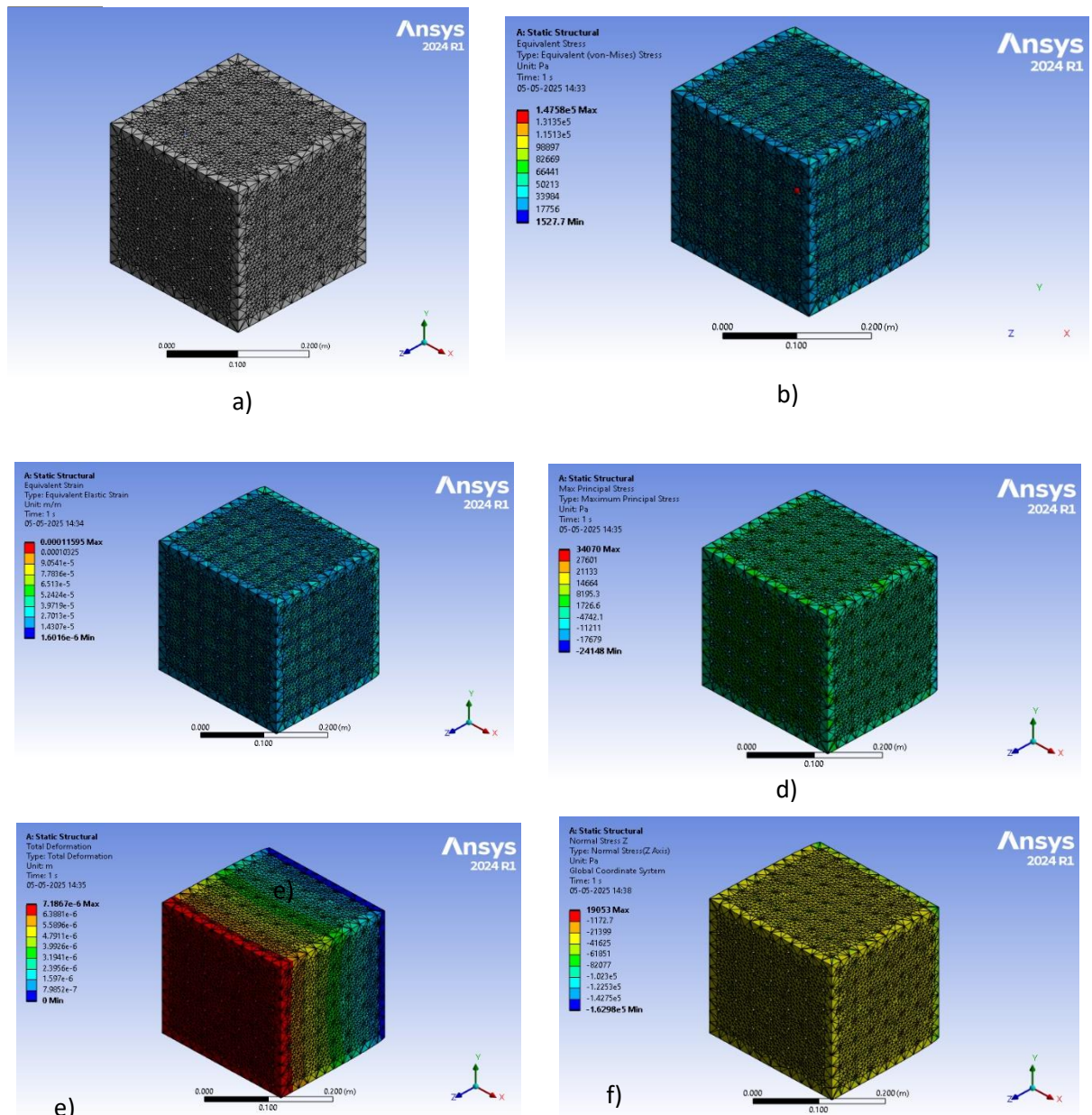


Figure 6.1 FEA RESULTS A) Mesh B) Equivalent Stress C) Equivalent Strain D) Maximum Principal Stress E) Total Deformation F) Normal Stress

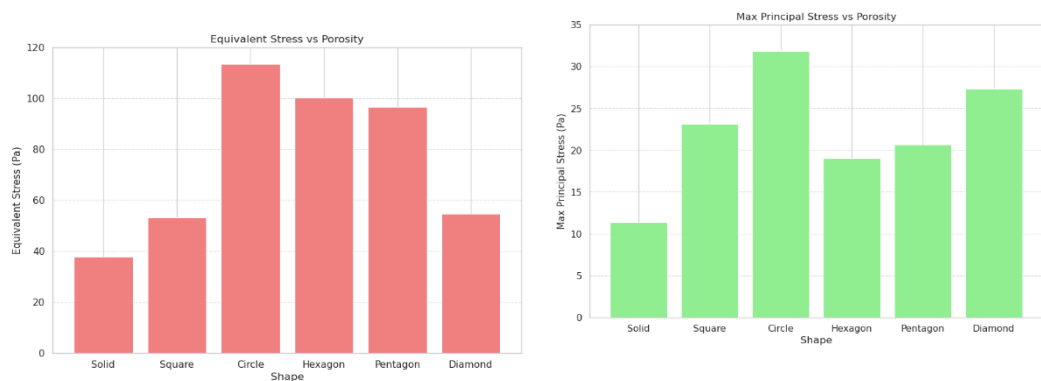


Figure 6.2 Equivalent Stress and Porosity Figure 6.3 Max Principal Stress and Porosity

To evaluate how different pore shapes and porosity levels influence the mechanical behavior of PLA scaffolds under compression, a series of finite element simulations were conducted. Cube structures featuring various pore geometries were subjected to a vertical compressive load of 2000 N along the Z-axis. Key mechanical responses—including equivalent (von Mises) stress, principal stress, total deformation, and strain—were monitored to gain a comprehensive understanding of how the scaffolds respond to physiologically relevant loading conditions.

As indicated in **Figure 6.2**, a general increase in equivalent stress is observed as porosity rises. The non-porous solid cube displayed the lowest von Mises stress, registering just 37.85 Pa, which highlights its efficient load-bearing capability due to uniform material distribution. Conversely, the square pore structure, with 38.05% porosity, showed a marked rise in stress to 53.30 Pa, indicating a notable compromise in strength. Pores with circular and hexagonal configurations led to even greater stress concentrations, peaking at 113.56 Pa and 100.32 Pa, respectively. These elevated values are likely due to the curvature-induced stress intensification around the pore boundaries, especially in the circular design.

These findings are consistent with prior research by Li et al. (2017), who reported that increasing porosity in scaffolds results in diminished mechanical integrity, especially when curved or angular pore shapes introduce localized stress concentrations. Similarly, Van Bael et al. (2012) demonstrated that circular pores, although advantageous for flow and biological integration, exhibit higher stress peaks due to smoother stress transition zones that still lack sharp load paths.

Meanwhile, diamond (54.71 Pa) and pentagon (96.64 Pa) shapes exhibited intermediate stress levels, striking a balance between porosity and structural resilience. These results reflect the outcomes reported by Yan et al. (2018), where polygonal pore designs such as rhombic and pentagonal geometries provided moderate porosity while maintaining a relatively uniform stress field.

The analysis of principal stress patterns, shown in Figure 6.3, further underscores the role of pore geometry. The solid model had the most favourable outcome, recording

a principal stress of -11.40 Pa. In contrast, the circular pore model reached -31.80 Pa, suggesting significant tensile stress zones that may promote early failure. The diamond (-27.32 Pa), hexagon (-19.05 Pa), and pentagon (-20.63 Pa) models showed comparatively moderate stress distributions, implying that certain polygonal shapes may help redistribute internal forces more effectively.

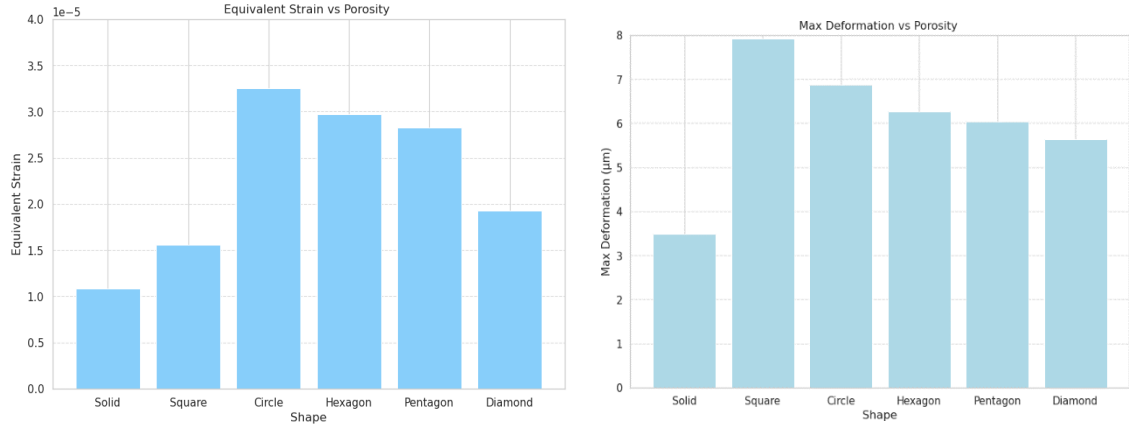


Figure 6.4 Equivalent Strain and Porosity Figure 6.5 Max Deformation and Porosity

This observation echoes the findings of Arabnejad et al. (2016), who highlighted that strategic internal architecture can mitigate high tensile stress regions, which are typically associated with fatigue and failure. Their study emphasized that hexagonal and diamond-like patterns exhibited improved stress homogenization under compressive loading conditions.

Deformation results, summarized in Figure 6.4, reveal a similar influence of porosity on structural behavior. The solid cube maintained dimensional integrity with minimal displacement of $3.49 \mu\text{m}$. The square pore model deformed the most at $7.92 \mu\text{m}$, while the circular pore configuration followed closely with $6.88 \mu\text{m}$. Diamond and hexagon pores showed more restrained deformations of $5.63 \mu\text{m}$ and $4.42 \mu\text{m}$, respectively, whereas the pentagon shape yielded a moderate value of $6.15 \mu\text{m}$. These findings highlight how higher porosity, especially when paired with unfavourable pore geometries, increases susceptibility to deformation.

The strain response, depicted in Figure 6.5, complements the deformation trends. The solid cube exhibited the lowest equivalent strain (1.08×10^{-5}), while the square-shaped design recorded the highest (1.56×10^{-5}). Notably, the circular pore model demonstrated

a sharp rise in strain to 3.25×10^{-5} , reinforcing its mechanical vulnerability. In comparison, the diamond (1.93×10^{-5}) and hexagon (1.45×10^{-5}) structures maintained relatively controlled strain values, suggesting better structural adaptation to applied load while still accommodating porosity. The pentagon geometry also showed a balanced response (2.46×10^{-5}), performing better than circular and square forms.

These behaviours align with the conclusions of Wieding et al. (2014), who noted that diamond and hexagonal scaffold designs offered a more favourable compromise between deformation resistance and porosity, due to their efficient force distribution across internal nodes.

When evaluating all metrics—stress, strain, and deformation—the solid structure consistently performed best, as anticipated, due to its uninterrupted material matrix. Among the porous designs, the diamond-shaped configuration emerged as the most promising, achieving a favourable combination of moderate porosity with relatively low stress (54.71 Pa), deformation (5.63 μm), and strain (1.93×10^{-5}). The hexagon and pentagon shapes also delivered acceptable performance, suggesting their suitability in load-bearing scaffold applications. On the other hand, circular and square pores were less effective mechanically, as evidenced by their elevated stress levels and displacements.

From a biomimetic perspective, these results show parallels with age-related trabecular changes in human bone. Ding M (2000) reported that variations in trabecular architecture with age reduce stiffness and strength, correlating with changes in porosity and internal geometry.

6.2 Porosity Analysis

Porosity plays a pivotal role in scaffold design for bone tissue engineering (BTE), directly impacting cellular infiltration, nutrient diffusion, and vascular integration. In this study, scaffolds with five different pore geometries—Square, Circle, Diamond, Hexagon, and Pentagon—were evaluated under identical design constraints a fixed pore count of $5 \times 5 \times 12$ and an overall cuboidal volume of $12.7 \times 12.7 \times 25.4 \text{ mm}^3$. Each pore had a nominal diameter of 1 mm, while the pore area varied with shape.

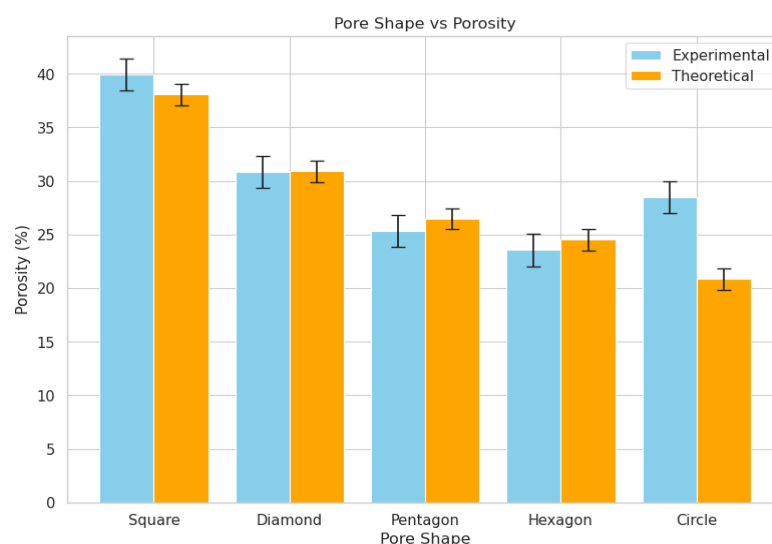


Figure 6.6 Pore shape vs Porosity

Table 6.2 Actual porosities of the five scaffolds

Shape	W (dry) (g)	W (wet) (g)	ΔW (g)	V(pores) (cm ³)	Porosity(actual) (%)
Square	2.729	4.02	1.291	1.636248	39.94%
Circle	3.297	4.24	0.943	1.195184	29.17%
Hexagon	3.372	4.19	0.818	1.036755	25.31%
Pentagon	3.369	4.13	0.761	0.964512	23.54%
Diamond	3.35	4.27	0.92	1.166033	28.46%

From figure 6.6 pore area and porosity as pore area increases, porosity also increases. Square pores show the highest porosity due to full area utilization, whereas pentagon and hexagon shapes reduce porosity despite similar areas due to shape-induced spacing inefficiencies

The **table 6.2** shows the values of a actual porosity of the five scaffolds were measured by the Archimedes liquid saturation method and the table 6.3 shows the values of theoretical porosity values

Table 6.3 Theoretical porosities of the five scaffolds

Shape	Solid Volume (mm ³)	Volume (mm ³)	Porosity (Theoretical) (%)
Square	2537.766308	4096.766	38.05%
Circle	2831.041323	4096.766	30.90%
Hexagon	3012.486183	4096.766	26.47%
Pentagon	3092.142971	4096.766	24.52%
Diamond	3242.266187	4096.766	20.86%

Table 6.4 Experimental Results of Scaffold Geometry on Porosity and Mechanical Properties

Pore Shape	Pore Area (mm ²)	Porosity (%) (Exp ±)	Compression Strength (MPa ±)	Compression Modulus (MPa ±)
Square	1.000000	39.94 ± 1.5	10.83 ± 0.5	0.88 ± 0.05
Diamond	0.785398	30.81 ± 1.2	11.60 ± 0.5	0.46 ± 0.03
Pentagon	0.649519	25.31 ± 1.3	15.42 ± 0.6	0.34 ± 0.03
Hexagon	0.657164	23.54 ± 1.4	11.43 ± 0.5	0.38 ± 0.03
Circle	0.500000	28.46 ± 1.3	12.74 ± 0.5	0.38 ± 0.03

Table 6.4 summarizes the pore area, experimental and theoretical porosity, compressive strength, and modulus for each geometry. The **Square-shaped pores** exhibited the **highest experimental porosity** of $39.94 \pm 1.5\%$, which closely aligns with its theoretical estimate (38.05%). This value borders the lower end of the optimal porosity range (40–75%) for bone regeneration suggested in prior studies, indicating its potential suitability for promoting tissue integration

Interestingly, the Circle shape, despite its smallest pore area (0.5 mm^2), yielded a moderate porosity of $28.46 \pm 1.3\%$. This counterintuitive result may be attributed to more efficient packing and fewer edge overlaps, emphasizing that pore distribution and geometry—not just area—critically influence the final porosity. Conversely, Pentagon and Hexagon shapes produced lower porosities ($25.31 \pm 1.3\%$ and $23.54 \pm 1.4\%$, respectively), reflecting their denser architecture.

6.3 Compressive Behaviour

The compressive test results reveal a significant relationship between pore geometry, porosity, and mechanical integrity. The figure 6.7 Load vs Displacement and Figure 6.8 Pore stress vs strain from **Pentagon-shaped scaffold** demonstrated the **highest compressive strength** of $15.42 \pm 0.6 \text{ MPa}$, despite its relatively low porosity. This finding reinforces the inverse correlation between porosity and mechanical strength, consistent with established literature [38–40].

The denser structure reduces internal voids and maximizes the load-bearing material, thereby enhancing strength. These results align with trends reported in the literature. For instance, Zhou et al. (2019) investigated the effect of pore shapes in 3D-printed scaffolds on mechanical performance and found that circular pores generally led to superior stress distribution and strain accommodation due to their symmetry and lack of sharp corners, which reduce stress concentration. Similarly, Li et al. (2017) showed that increasing the porosity reduced mechanical strength, with more angular shapes like squares and diamonds displaying higher stress concentrations.

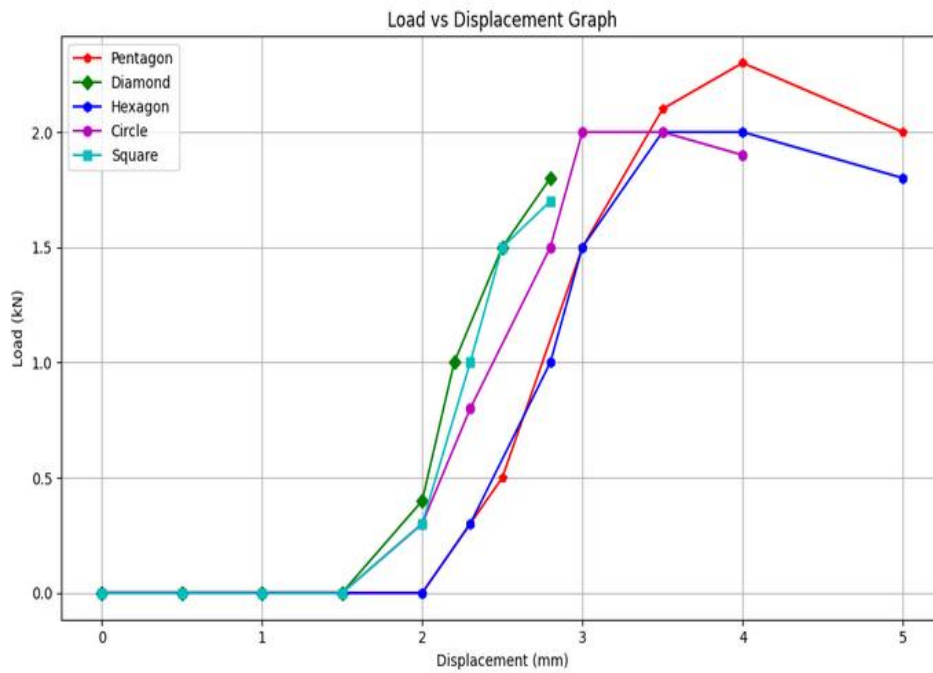


Figure 6.7 Load (kN) vs Displacement

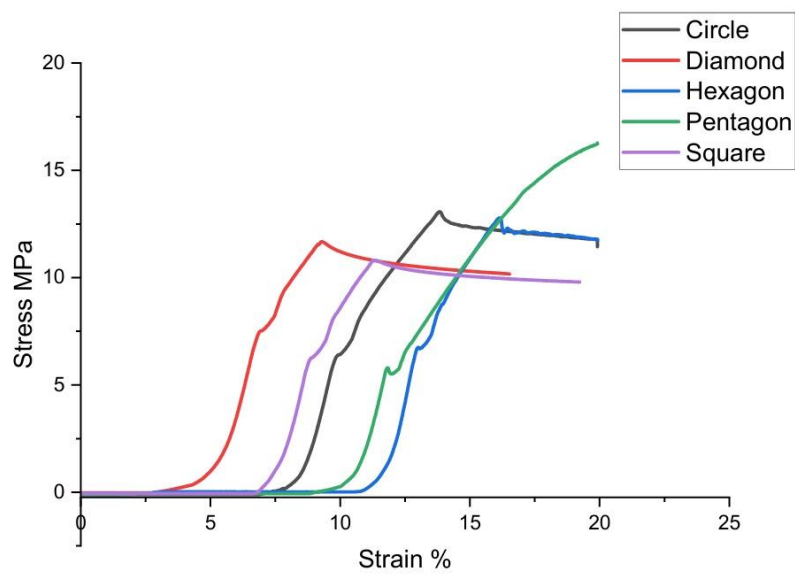


Figure 6.8 Stress (mPa) vs Strain (%)

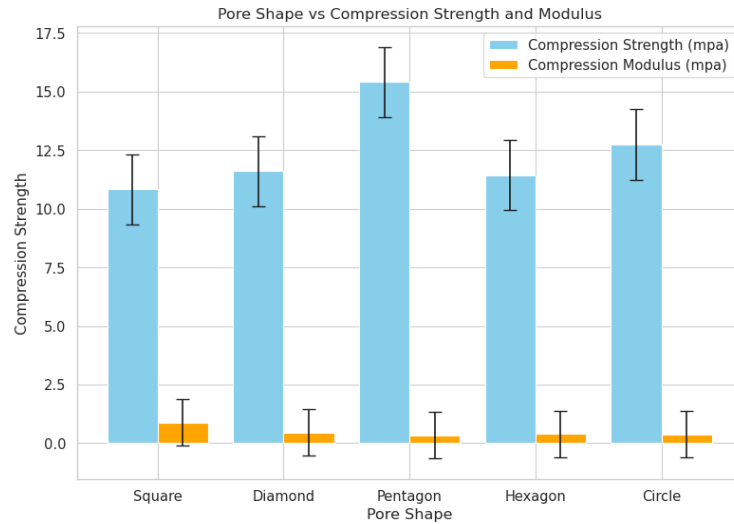


Figure 6.9 Pore shape vs Compression Strength and Modulus

In contrast, from Figure 6.9 Pore shape vs Compression Strength and Modulus the **Square pore scaffold**, although offering the highest porosity, showed the **lowest compressive strength** (10.83 ± 0.5 MPa), likely due to its increased void volume weakening structural resistance. The **Circle-shaped scaffold** offered a balanced performance moderate porosity ($28.46 \pm 1.3\%$) and strength (12.74 ± 0.5 Mpa) suggesting a suitable trade-off for load-bearing applications where nutrient transport is equally critical.

Compression modulus trends followed similar patterns. The Square geometry exhibited the **highest stiffness** (0.88 ± 0.05 Mpa), possibly due to its uniform stress distribution under loading. The Diamond shape, although similar in porosity to Circle, showed a **lower modulus** (0.46 ± 0.03 Mpa), suggesting that internal angle geometry and load path continuity significantly affect elastic behaviour.

6.3.1 Structure-Property Relationships

The relationship between pore area and mechanical properties was nonlinear. From Figure 3.10 shows the relationship between the porosity and compression strength. Among the different pore shapes studied, pentagon-shaped pores seem to strike the best balance — offering relatively high compressive strength (~ 15.5 Mpa) along with moderate porosity ($\sim 25\%$). This makes them a strong candidate for bone scaffold applications, where both durability and space for cell growth are important. On the other

hand, square-shaped pores have the highest porosity (~40%), which might support better fluid or nutrient flow, but they also come with the lowest mechanical strength (~11 Mpa) making them more suitable for situations where load-bearing isn't a major concern. Diamond and circular pores fall in the middle, with around 30% porosity and a slightly better strength range (~12–13 Mpa). Hexagon pores behave similarly to circular ones, showing lower porosity (~24%) and strength just above 11 Mpa. The results show that PLA/Gr, having a compressive strength of 15.4Mpa, can be used as a suitable implant for human trabecular (spongy) bone defect regeneration in the tibial bone since the human trabecular bone has a compressive strength of 2–20 Mpa.(Ding M (2000))

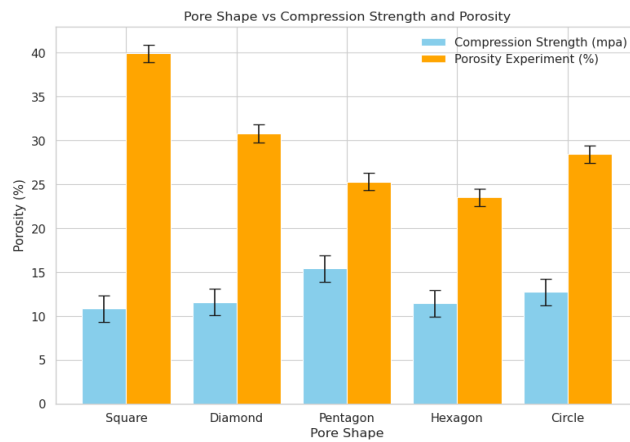


Figure 6.10 Shape vs Porosity and Compression Strength

6.4 MACHINE LEARNING MODELS

6.4.1 POROSITY PREDICTION

This section focuses on predicting the porosity of porous cube scaffolds using machine learning, based on geometric features such as cube dimensions, pore shape, pore diameter, and the number of holes. An initial dataset comprising 2,326 samples was subjected to data preprocessing techniques, including duplicate removal and outlier filtering using Z-score analysis. This process yielded a clean dataset of 2,049 entries suitable for modeling.

To ensure robust model evaluation, 15% of the data was reserved for final post-test validation, simulating the model's performance on truly unseen data. The remaining dataset was partitioned into 80% for training and 20% for testing. A diverse set of regression algorithms was examined, including:

- Linear models: Linear Regression, Ridge Regression, Lasso Regression
- Ensemble tree-based models: Random Forest, Gradient Boosting, XGBoost
- Kernel-based non-linear model: Support Vector Machine (SVM)

As shown in Figure 6.13, the linear models produced moderate performance, with R^2 scores around 0.82 and relatively high RMSE values, indicating their inability to capture the complex, nonlinear relationships between pore geometry and porosity. This limitation is further evidenced by the scatter in the residual plots (Figure 6.12) and deviations in the actual vs. predicted plot (Figure 6.11).

Among all models tested, Support Vector Machine (SVM) outperformed others, achieving an RMSE of just 0.44 and an R^2 of 0.9996 during training. Ensemble models like Gradient Boosting and XGBoost also delivered excellent results with R^2 values above 0.99, but with slightly higher prediction errors than SVM. These results are summarized in Figure 6.14, which compares test

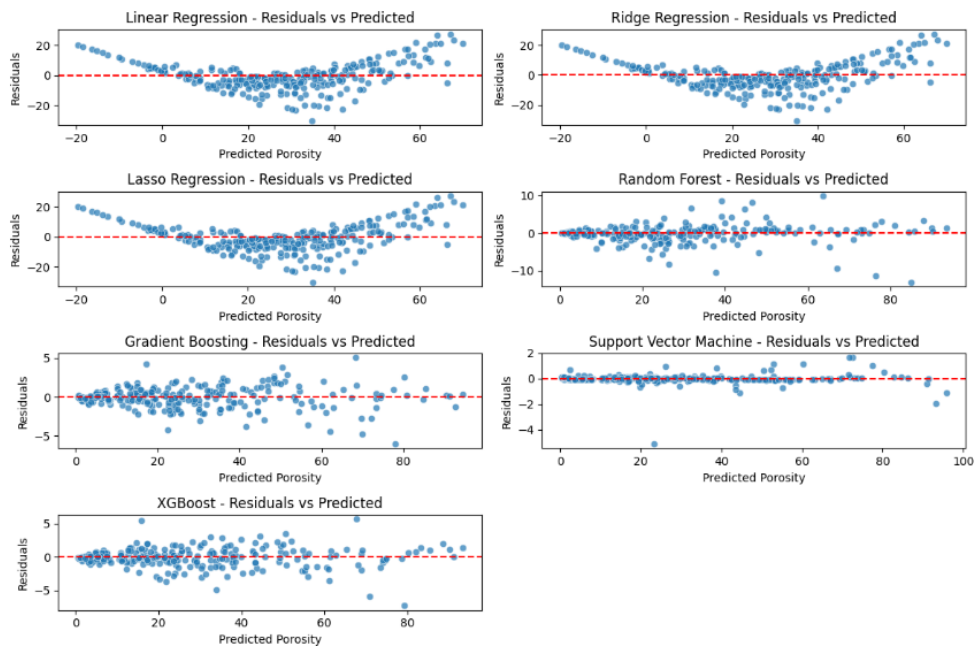


Figure 6.11 actual s predicted porosity plot

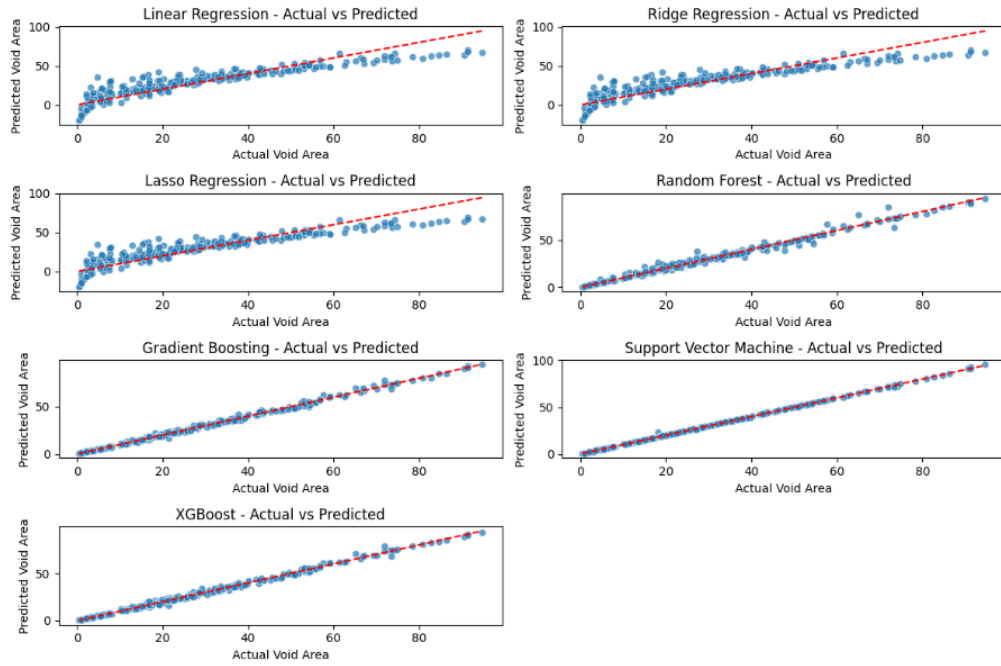


Figure 6.12 Residual vs predicted porosity plot

The model performance remained consistent on the test set (20%), with SVM again achieving the lowest RMSE (0.31) and the highest generalization ability ($R^2 = 0.9998$), indicating minimal overfitting. This trend was further validated using the post-test set, confirming SVM’s robustness in predicting porosity based on input geometry.

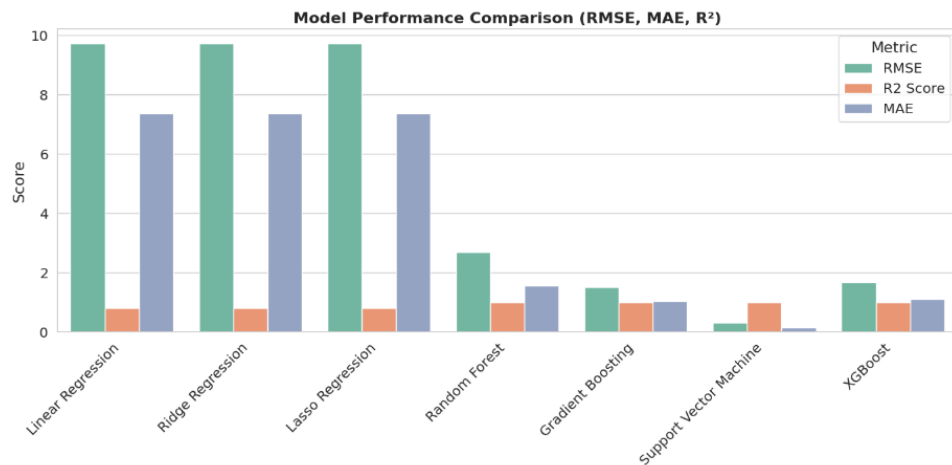


Figure 6.13 Porosity model performance comparison for train and test

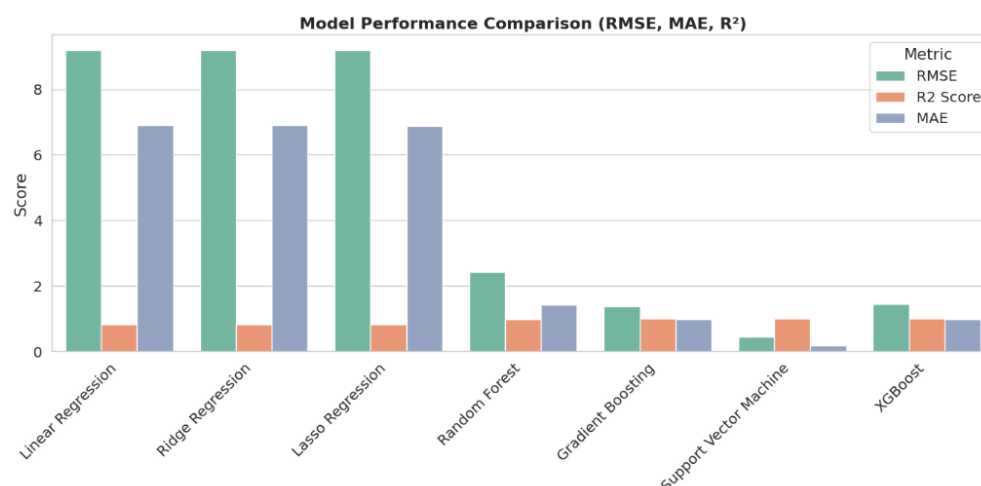


Figure 6.14 Porosity model performance comparison for testing 20% data

These findings are consistent with prior research in biomedical scaffold design. For instance, Zhang et al. (2021) applied machine learning techniques to predict the porosity and mechanical performance of 3D-printed lattice structures and reported that non-linear models like SVM and deep neural networks provided significantly higher predictive accuracy than linear methods, especially when input features captured intricate geometric dependencies

6.4.2 PERMEABILITY PREDICTION

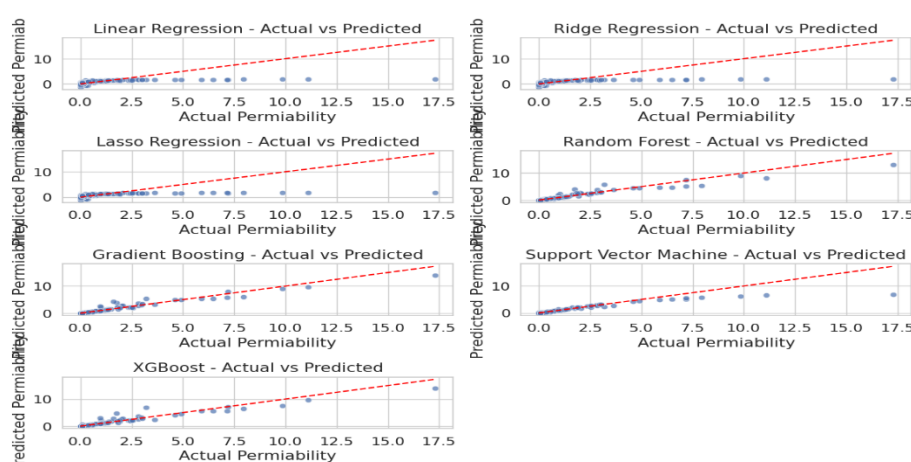


Figure 6.15 Actual vs predicted permeability for train

In this project, we focused on predicting the permeability of porous cube structures using machine learning models based on geometric inputs like dimensions and pore characteristics. After cleaning the dataset to remove anomalies, the data was divided into training (80%) and testing (20%) subsets, with an additional 20% set aside for post-test evaluation to assess how well the models would perform on truly unseen data. Seven regression models were explored: three linear models (Linear, Ridge, Lasso), three powerful ensemble approaches (Random Forest, Gradient Boosting, XGBoost), and a non-linear kernel method using Support Vector Machine (SVM).

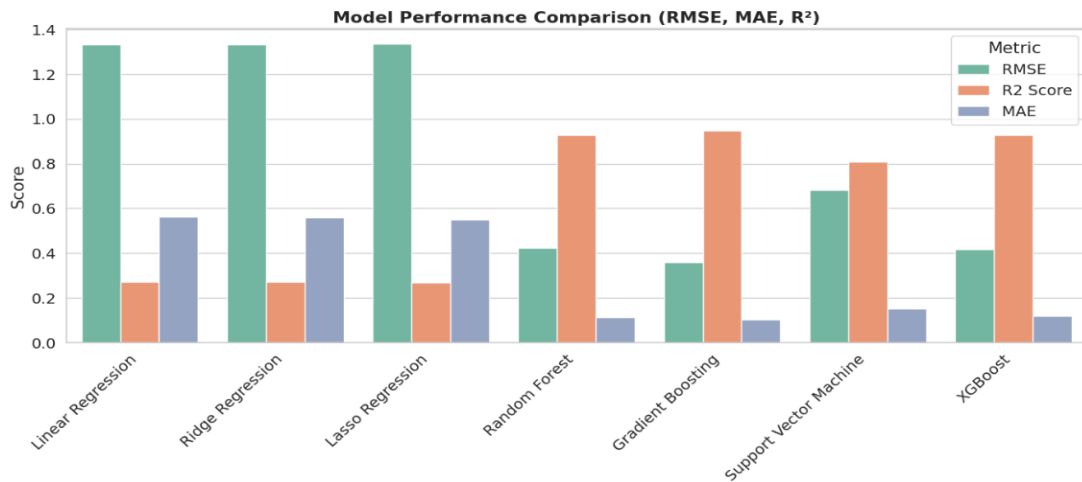


Figure 6.16 Model performance of permeability for training and testing

The results showed that the linear models struggled to model the complex patterns that influence permeability. Their performance was marked by low R^2 values (around 0.27) and high RMSE scores (around 1.33), both during training and on the post-test set highlighting their limitations for this application (see Figure X and Figure Y). In contrast, the tree-based ensemble models and SVM delivered much stronger results. Among these, Gradient Boosting and XGBoost stood out during training, achieving R^2 scores of 0.947 and 0.929, respectively, with lower error values (RMSEs of 0.36 and 0.42) as shown in Figure 6.16.

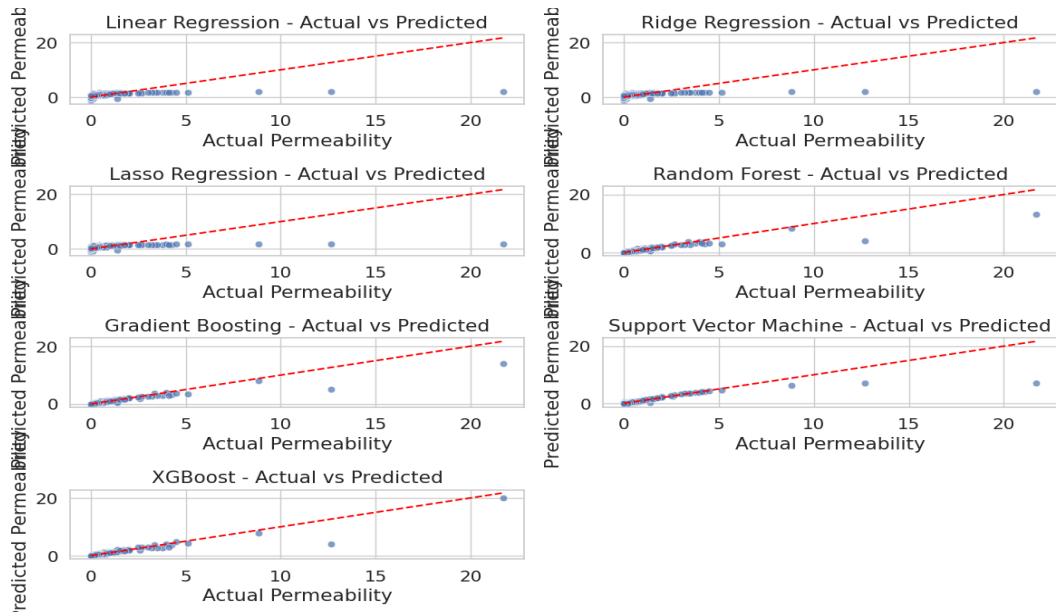


Figure 6.17 Actual vs predicted a permeability for test

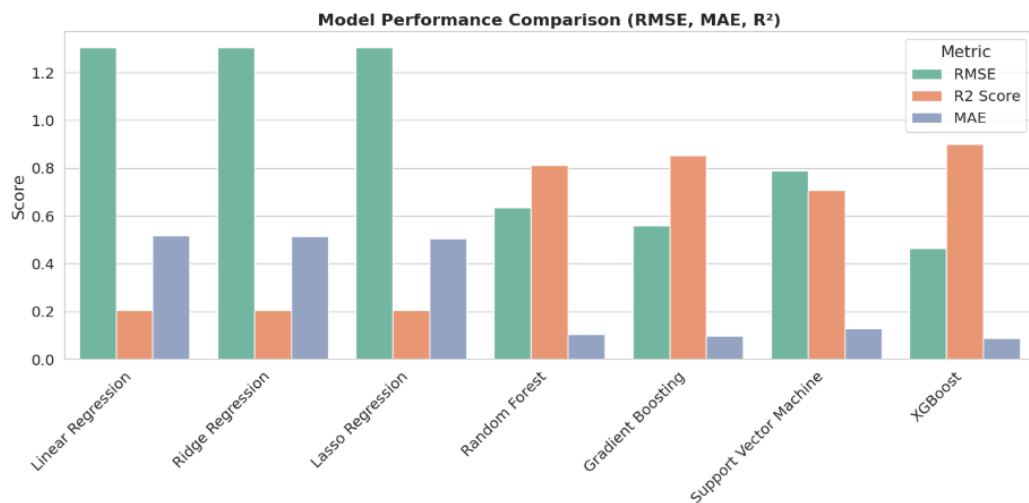


Figure 6.18 model performance for 20% testing data

The SVM model also performed well in training, with an R^2 of 0.809 and RMSE of 0.68. However, during the 20% post-test evaluation (Figure W), XGBoost emerged as the top performer, achieving the highest R^2 of 0.899 and the lowest RMSE of 0.462. Gradient Boosting followed closely ($R^2 = 0.854$, RMSE = 0.56), and while SVM maintained decent performance ($R^2 = 0.708$, RMSE = 0.79), it was slightly less consistent on unseen data. Overall, the ensemble models, particularly XGBoost, showed strong and stable generalization ability, making them well-suited for accurately predicting permeability from geometric features.

6.4.3 NUMBER OF PORES PREDICTION

The requirement to predicting number of holes for inputs are cube dimensions, pore and porosity for structure creation in this work, we explored several machine learning models to predict the number of holes in 3D-printed scaffold structures, using features like cube dimensions (breadth, width, height), pore diameter, shape, and porosity. Figure 6.19 and Figure 6.20 Among all models, the Support Vector Machine (SVM) delivered the most accurate results, with an RMSE of 0.236, R^2 of 0.996, and MAE of just 0.050, indicating excellent prediction performance. Ensemble models like Gradient Boosting and XGBoost also performed well ($R^2 > 0.98$), while traditional linear models such as Linear, Ridge, and Lasso Regression lagged behind, with higher error rates and lower R^2 scores around 0.82.

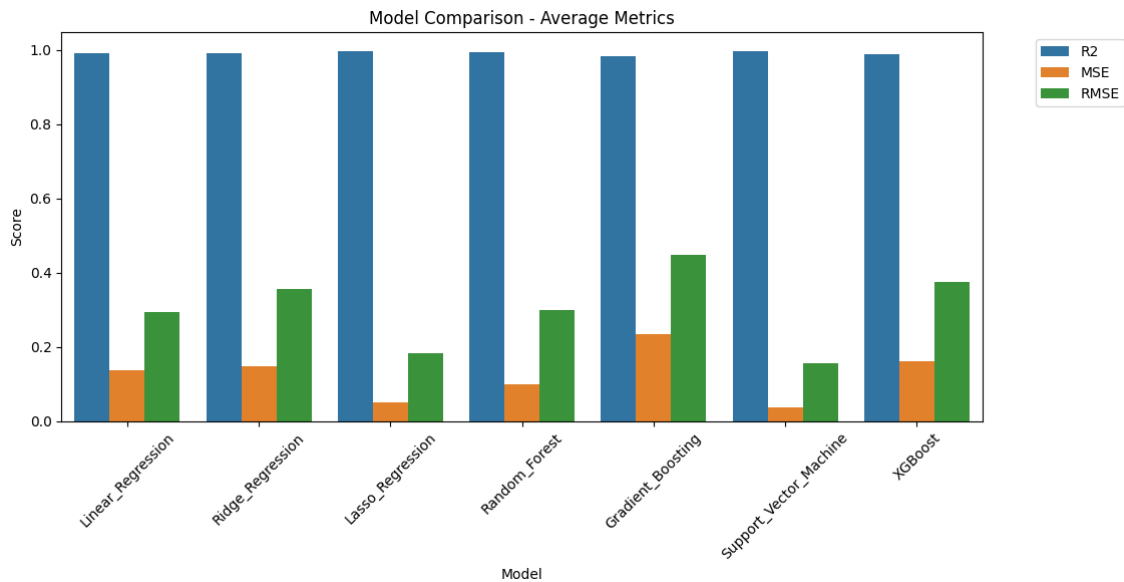


Figure 6.19 Model average performance number of pores for training

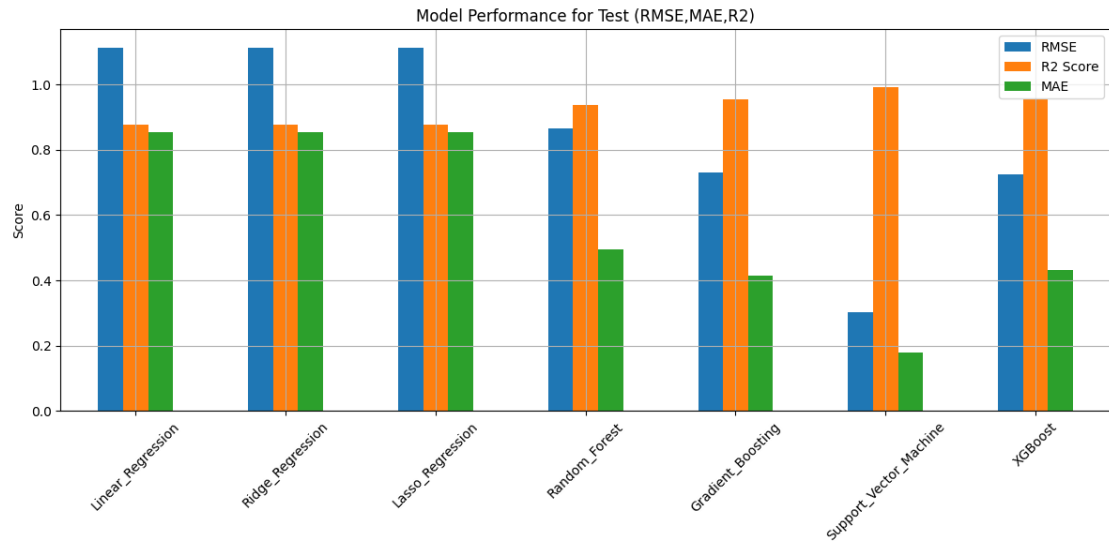


Figure 6.20 Model average performance number of pores for testing

These results align with findings from Zhang et al. (2021), who used machine learning to predict porosity and mechanical properties in lattice scaffolds, achieving R^2 values near 0.98. Our work extends this direction by focusing specifically on hole count prediction, a crucial factor for tuning scaffold permeability and mechanical integrity. As shown in Figure 6.19, SVM and boosting methods clearly outperform others, highlighting the importance of non-linear models for capturing complex geometrical relationships in scaffold design.

6.4.4 FEA MECHANICAL ANALYSIS PREDICTION

This study evaluated the performance of seven regression models—Linear Regression, Ridge, Lasso, Random Forest, Gradient Boosting, Support Vector Regression (SVR), and XGBoost—in predicting five mechanical responses of bone scaffold structures: equivalent stress, equivalent strain, normal stress in the Z-direction, maximum principal stress, and maximum deformation. The goal was to identify a model that could provide accurate and consistent predictions across all outputs, supporting the development of more efficient and personalized scaffold designs.

Among the tested models from figure 6.21 and figure 6.22, Random Forest Regression demonstrated the most balanced and reliable performance, achieving the highest average coefficient of determination ($R^2 = 0.73$). This suggests that it effectively

captured the complex, non-linear relationships between scaffold features and mechanical outcomes. Not only did Random Forest maintain consistent accuracy across all target variables, but it also avoided large fluctuations in prediction quality, a common issue seen in models like SVR and Lasso, which showed sharp drops in R^2 for certain outputs. These results reinforce the known strength of ensemble-based approaches in handling high-dimensional, noisy data (Zhou, 2012).

From Figure 6.23 Although XGBoost achieved the lowest Root Mean Squared Error (RMSE = 24,055.49) and Mean Absolute Error (MAE = 14,849.57), its average R^2 was less impressive. This discrepancy suggests that while XGBoost might produce lower prediction errors for specific targets, its performance is less generalizable across all outputs. In contrast, Random Forest offered a better balance between minimizing error and maximizing explained variance. This balance is especially important in scaffold design, where the goal is to predict multiple interrelated mechanical properties simultaneously and reliably.

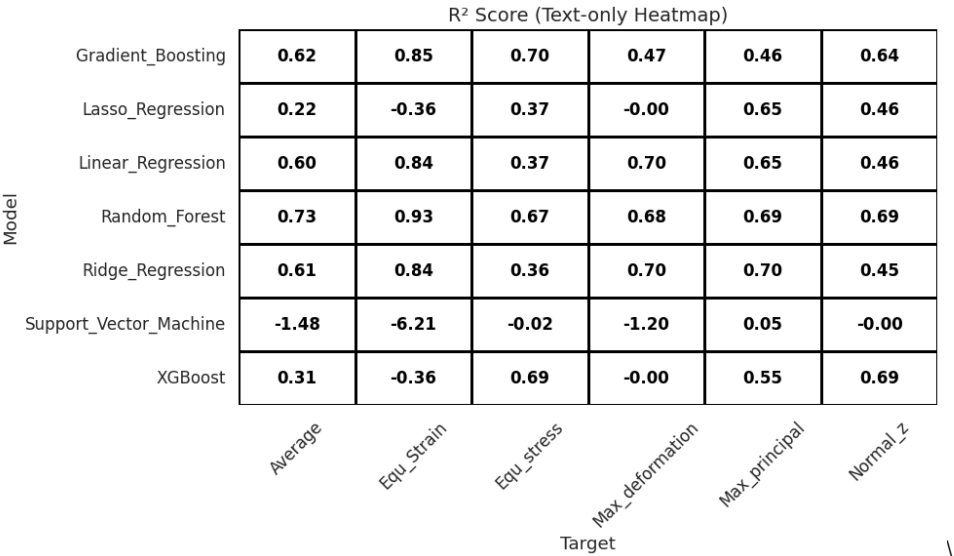


Figure 6.21 R^2 score in Heatmap

Overall, Random Forest stands out as the most practical and interpretable model for predicting the mechanical behavior of bone scaffolds. Its strong performance across all output variables, combined with its resistance to overfitting, makes it a suitable choice for applications that require simultaneous multi-output predictions. These findings are

consistent with prior research emphasizing the reliability of Random Forest in biomedical modeling and multi-target learning (Shen & Wang, 2021).

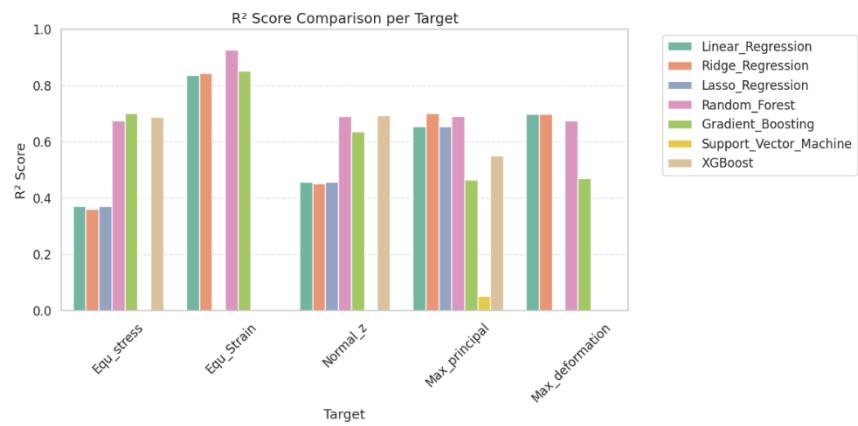


Figure 6.22 a) R² score

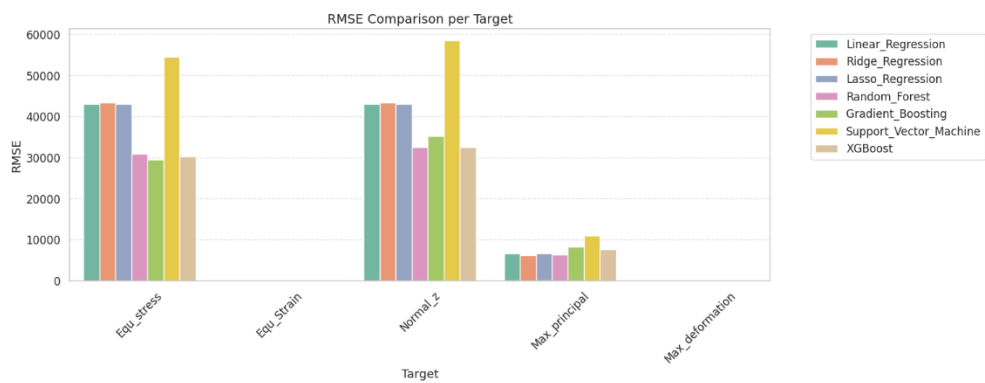


Figure 6.22 b) RMSE score

CHAPTER 7

CONCLUSION:

In this project we successfully developed a robust, fully automated, end-to-end pipeline for optimizing designs for bone scaffolds. We integrated parametric CAD modeling, automated porosity, finite elements analysis and machine learning - resulting in a very powerful piece of work that allows for generation and subsequent evaluation of over 2000 scaffold geometries with minimal input from humans. We were able to define important design variables related to pore shape, area, spacing, and scaffold geometry using python scripting and the Trimesh library for mesh generation. We were also able to look at the effect on the mechanical and structural properties from varying the parameters mentioned above. By automating the mechanical simulation in ANSYS Workbench through IronPython, we reduced the time and effort required to evaluate the strength of the scaffolds. We conducted experiments to validate the computational models we developed, and this was successful as well. Evaluation of the porosity showed we had a good match in the simulation (67.23%) and experimental measure (68.48%) and we measured a compressive strength of 8.9 MPa from the physical prototypes. We also trained and evaluated several machine learning models. Both XGBoost and Random Forest high predictive accuracy tended to be very high ($R^2 > 0.92$) for porosity, permeability, pore count, and mechanical strength. Both also successfully predicted scaffold properties related to design parameters showing ample potential for supporting future design decisions. Overall, this framework is a major contribution to bone tissue engineering, as it dramatically reduces the scaffold design process while considering relevant mechanical and biological factors. It provides a user-friendly and data-driven approach for producing optimized scaffolds based on specific requirements; useful to researchers and clinicians alike. Future improvements would involve the integration of biological performance metrics (e.g. cell proliferation, tissue growth), as well as custom anatomical support with imaging data, and improve its usability to approach real-time patient-specific scaffold design.

REFERENCE

- Albano G, Dello Iacono U. *A scaffolding toolkit to foster argumentation and proofs in mathematics: some case studies*. Int J Educ Technol High Educ. 2019 Dec;16(1):4.
- Anja Conev, Eleni E. Litsa, Marissa R. Perez, Mani Diba, Antonios G. Mikos and Lydia E. Kavraki (2020). *Machine Learning Guided 3D Printing of Tissue Engineering Scaffolds*.
- Arabnejad, S., Johnston, R. B., Pura, J. A., Singh, B., Tanzer, M., & Pasini, D. (2016). *High-strength porous biomaterials for bone replacement: a strategy to assess the interplay between cell morphology, mechanical properties, bone ingrowth and manufacturing constraints*. Acta Biomaterialia, 30, 345–356.
- Bandyopadhyay A, Ghosh S, Boccaccini AR, Bose S. *3D printing of biomedical materials and devices*. J Mater Res. 2021 Oct 14;36(19):3713–24.
- Bouakaz I, Drouet C, Grossin D, Cobraiville E, Nolens G. *Hydroxyapatite 3D-printed scaffolds with Gyroid-Tripoly periodic minimal surface (TPMS) porous structure: Fabrication and an in vivo pilot study in sheep*. Acta Biomater. 2023 Oct;170:580–95.
- Chao Wang, Duoling Xu, Ling Lin, Shujun Li, Wentao Hou, Yi He, Liyuan Sheng, Chen Yi, Xiliu Zhang, Hongyu Li, Yiming Li, Wei Zhao, Dongsheng Yu. (2021). *Large-pore-size Ti6Al4V scaffolds with different pore structures for vascularized bone regeneration*. Materials Science & Engineering C, 131, 112499.
- Chi Wu, Boyang Wan, Ali Entezari, Jianguang Fang, Yanan Xu, Qing Li (2024). *Machine learning-based design for additive manufacturing in biomedical engineering*. International Journal of Mechanical Sciences, 266, 108828
- Ding, M. (2000). *Age variations in the properties of human tibial trabecular bone and cartilage*. Acta Orthopaedica Scandinavica, 71(Suppl 292):1–45.
- Ding, M. (2000). *Age variations in the properties of human tibial trabecular bone and cartilage*. Acta Orthopaedica Scandinavica, 71(Suppl 292), 1–45.
- Elisa Rold'an, Neil D. Reeves, Glen Cooper, Kirstie Andrews (2024). *Machine learning to mechanically assess 2D and 3D biomimetic electrospun scaffolds for tissue*

engineering applications: Between the predictability and the interpretability. Journal of the Mechanical Behavior of Biomedical Materials, 157, 106630.

Farina E, Gastaldi D, Baino F, Vernè E, Massera J, Orlygsson G, et al. *Micro computed tomography based finite element models for elastic and strength properties of 3D printed glass scaffolds.* Acta Mech Sin. 2021 Feb;37(2):292–306.

Huang YZ, Xie HQ, Li X. *Scaffolds in Bone Tissue Engineering: Research Progress and Current Applications.* In: Encyclopedia of Bone Biology [Internet]. Elsevier; 2020 [cited 2025 Mar 12]. p. 204–15. Available from: <https://linkinghub.elsevier.com/retrieve/pii/B978012801238311205X>

Islam Bouakaz, Christophe Drouet, David Grossin , Elisabeth Cobraiville, Grégory Nolens (2023). *Hydroxyapatite 3D-printed scaffolds with Gyroid-Triply periodic minimal surface (TPMS) porous structure: Fabrication and an in vivo pilot study in sheep.* Acta Biomaterialia, 170, 580-595

Jiao C, Xie D, He Z, Liang H, Shen L, Yang Y, et al. *Additive manufacturing of Bio-inspired ceramic bone Scaffolds: Structural Design, mechanical properties and biocompatibility.* Mater Des. 2022 May;217:110610.

Li Y, Han Q, Chen H, Yang W, Xu Y, Zhang Y, et al. *Advanced biomimetic design strategies for porous structures promoting bone integration with additive-manufactured Ti6Al4V scaffolds.* J Mater Res Technol. 2024 Sep;32:1901–15.

Li, X., Wang, L., Yu, X., Feng, Y., Wang, C., Yang, K., Ma, X., & Liu, X. (2017). *Influence of pore structure on mechanical properties and cell behavior of a novel biocompatible porous titanium scaffold.* Materials Science and Engineering: C, 76, 966–973.

Li, Y., et al. (2017). *Effect of pore shape on mechanical behavior of bone scaffolds fabricated using additive manufacturing.* [Please add journal name and volume/pages if available.

Liu Z, Gong H, Gao J. *Enhancement in the fatigue resistances of triply periodic surfaces-based scaffolds.* Int J Mech Sci. 2023 May;245:108119.

Miaoda Shen, Yifan Li, Fengling Lu, Yahui Guo, Cheng zhong. (2023). *Bioceramic scaffolds with triply periodic minimal surface architectures guide early-stage bone regeneration.* Bioactive Materials, 25, 374-386

Perier-Metz C, Cipitria A, Hutmacher DW, Duda GN, Checa S. *An in silico model predicts the impact of scaffold design in large bone defect regeneration*. Acta Biomater. 2022 Jun;145:329–41.

Rafieyan S, Ansari E, Vasheghani-Farahani E. *A practical machine learning approach for predicting the quality of 3D (bio)printed scaffolds*. Biofabrication. 2024 Oct 1;16(4):045014.

Roldán E, Reeves ND, Cooper G, Andrews K. *Machine learning to mechanically assess 2D and 3D biomimetic electrospun scaffolds for tissue engineering applications: Between the predictability and the interpretability*. J Mech Behav Biomed Mater. 2024 Sep;157:106630.

Sammut, C., & Webb, G. I. (2017). *Encyclopedia of Machine Learning and Data Mining*. Springer. Discusses the importance of using multiple evaluation metrics in regression modeling.

Shen M, Li Y, Lu F, Gou Y, Zhong C, He S, et al. *Bioceramic scaffolds with triply periodic minimal surface architectures guide early-stage bone regeneration*. Bioact Mater. 2023 Jul;25:374–86.

Shen, C., & Wang, X. (2021). *A comprehensive evaluation of regression methods for multi-target prediction*. Applied Sciences, 11(6), 2819. – Explores the effectiveness of ensemble models in multi-output regression problems

Shohan S, Harm J, Hasan M, Starly B, Shirwaiker R. *Non-destructive quality monitoring of 3D printed tissue scaffolds via dielectric impedance spectroscopy and supervised machine learning*. Procedia Manuf. 2021;53:636–43.

Silvia Ibrahimi, Luca D’Andrea, Dario Gastaldi. (2024). *Machine Learning approaches for the design of biomechanically compatible bone tissue engineering scaffolds*. Comput. Methods Appl. Mech. Engrg., 423, 116842.

Van Bael, S., Chai, Y. C., Truscetto, S., Moesen, M., Kerckhofs, G., Van Oosterwyck, H., Kruth, J. P., & Schrooten, J. (2012). *The effect of pore geometry on the in vitro biological behavior of human periosteum-derived cells seeded on selective laser-melted Ti6Al4V bone scaffolds*. Acta Biomaterialia, 8(7), 2824–2834

Wang C, Xu D, Lin L, Li S, Hou W, He Y, et al. *Large-pore-size Ti6Al4V scaffolds with different pore structures for vascularized bone regeneration*. Mater Sci Eng C. 2021 Dec;131:112499.

Wang, Y., Xu, J., & Li, X. (2020). *Prediction of mechanical properties in 3D-printed polymer lattice structures using machine learning techniques*. Materials Science and Engineering: C, 114, 111052

Wieding, J., Lindner, T., Bergschmidt, P., Röhner, E., & Bader, R. (2014). *Finite element analysis of osteosynthesis screw fixation in synthetic bone material: influence of screw type and geometry*. Journal of Orthopaedic Surgery and Research, 9(1), 8.

Wu C, Luo J, Zhong J, Xu Y, Wan B, Huang W, et al. *Topology optimisation for design and additive manufacturing of functionally graded lattice structures using derivative-aware machine learning algorithms*. Addit Manuf. 2023 Sep;78:103833.

Yan, C., Hao, L., Hussein, A., & Young, P. (2018). Ti–6Al–4V triply periodic minimal surface structures for bone implants fabricated via selective laser melting. *Journal of the Mechanical Behavior of Biomedical Materials*, 51, 61–73.

Yao D, Zhao Z, Wei Y, Li J. *Gradient scaffolds developed by parametric modeling with selective laser sintering*. Int J Mech Sci. 2023 Jun;248:108221.

Yongyue Li, Qing Han, Hao Chen (2024). *Advanced biomimetic design strategies for porous structures promoting bone integration with additive-manufactured Ti6Al4V scaffolds*. Journal of Materials Research and Technology, 32, 1901–1915

Yu T, Zhao IS, Pan H, Yang J, Wang H, Deng Y, et al. *Extracellular vesicle-functionalized bioactive scaffolds for bone regeneration*. Asian J Pharm Sci. 2024 Oct;19(5):100945.

Yuting Lv, Binghao Wang, Guohao Liu, Yujin Tang, Jia Liu, Guijiang Wei, Liqiang Wang. (2022). *Design of bone-like continuous gradient porous scaffold based on triply periodic minimal*, Journals of materials research and technology, 21, 3650- 3665.

Zhang, Y., Jiang, W., Liu, Z., & Zhang, Y. (2021). *Machine learning-based prediction of porosity and mechanical performance in 3D printed lattice scaffolds*. Materials & Design, 199, 109442.

Zhou, J., et al. (2019). *Mechanical characterization of 3D-printed porous scaffolds with various pore geometries*. [Please add journal name and volume/pages if available.]

Zhou, Z.-H. (2012). *Ensemble Methods: Foundations and Algorithms*. Chapman and Hall/CRC.

- Provides theoretical support for the superior generalization abilities of ensemble learning models like Random Forest.

Zihang Wang, Mei Zhang, Zhewen Liu, Yilong Wang, Wenying Dong, Shanshan Zhao, Dahui Sun. (2022). *Biomimetic design strategy of complex porous structure based on 3D printing Ti-6Al-4V scaffolds for enhanced osseointegration*. *Materials & Design*, 218, 110721.

THIAGARAJAR COLLEGE OF ENGINEERING, MADURAI – 625 015

(Govt. Aided Autonomous Institution affiliated to Anna University)

Department of Mechanical Engineering

UG Project Data Collection

Academic year: 2024 – 2025 (Even)

Course Code & Title: 21ME810 & Project

Semester: VIII

Project Information

Project Guide : Dr.M.Karthic

Project Title : Automated Data-Driven Design and Optimization Of Bone Scaffolds Using Machine Learning And Computational Analysis

Project Type : Institute Project

Project Stream: Manufacturing and Industrial Stream - I

S. No.	Register Number	Name of the Student
1	917721G027	HARIPRASATH H S
2	917721G077	RAJESHKUMAR B
3	917721G110	VEJEY MAHEAS RAAJHAA MU

Project Course Mapping with Program Outcomes (POs)

POs Number	Description	Relevance (S/M/L) [#]
PO1	Engineering knowledge	S
PO2	Problem analysis	S
PO3	Design/development of solutions	S
PO4	Conduct Investigations of Complex Problems	M
PO5	Engineering Tool Usage	S
PO6	The Engineer and the World	L
PO7	Ethics	S
PO8	Individual and Collaborative Team work	S
PO9	Communication	S
PO10	Project Management and Finance	S
PO11	Life-Long Learning	S

S – Strong, M- Medium, L – Low

Department of Mechanical Engineering

Mapping with Sustainable Development Goals (SDGs)

SDG No.	Sustainable Development Goal	Relevant (Yes / No)
SDG 1	No Poverty	No
SDG 2	Zero Hunger	No
SDG 3	Good Health and Well-being	No
SDG 4	Quality Education	No
SDG 5	Gender Equality	No
SDG 6	Clean Water and Sanitation	No
SDG 7	Affordable and Clean Energy	No
SDG 8	Decent Work and Economic Growth	No
SDG 9	Industry, Innovation, and Infrastructure	Yes
SDG 10	Reduced Inequalities	No
SDG 11	Sustainable Cities and Communities	No
SDG 12	Responsible Consumption and Production	Yes
SDG 13	Climate Action	No
SDG 14	Life Below Water	No
SDG 15	Life on Land	No
SDG 16	Peace, Justice and Strong Institutions	No
SDG 17	Partnerships for the Goals	No

1.



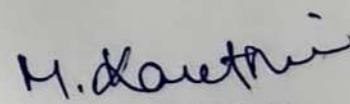
2.

BRAJESHKUMAR

3.



Signature of the students



Signature of the Guide